UNIVERSITY OF OKLAHOMA

GRADUATE COLLEGE

CHARACTERISTICS AND LIFECYCLES OF ANTICYCLONIC TROPOPAUSE POLAR VORTICES

A THESIS

SUBMITTED TO THE GRADUATE FACULTY

in partial fulfillment of the requirements for the

Degree of

MASTER OF SCIENCE

By

JOSEPH BURZDAK
Norman, Oklahoma
2023

CHARACTERISTICS AND LIFECYCLES OF ANTICYCLONIC TROPOPAUSE POLAR VORTICES

A THESIS APPROVED FOR THE
SCHOOL OF METEOROLOGY

BY THE COMMITTEE CONSISTING OF

Dr. Steven Cavallo (Chair)

Dr. David Parsons

Dr. Jason Furtado

Acknowledgments

I would like to thank my advisor Dr. Steven Cavallo for all of your help throughout this research as well as your care and understanding as I adjusted to graduate school during the Covid pandemic. I also thank you for your continuous support through the update and following complications with the Arctic server. I would also like to thank my co-advisor Dr. David Parsons for your help in preparing the research and all the presentations I have given while here at OU. I thank Dr. Jason Furtado for being on my committee and for your help to edit and prepare this thesis. I want to also thank the entire AAARG team for helpful meetings each week and insightful suggestions about how to execute this research. Finally, I thank all my family and friends for their love and support as I prepared this research and overcame obstacles related to moving away from home, the Covid pandemic, and other personal adversities. I would not have been able to accomplish this without you.

Table of Contents

List Of Figures

Abstract

Tropopause polar vortices (TPVs) are sub-synoptic, long-lived, closed circulation features located in the upper-troposphere and lower-stratosphere region. Although TPV circulations can be cyclonic or anticyclonic, most previous studies have focused only on cyclonic TPVs, especially due to their direct influence on weather systems, including Arctic cyclones, but also cold air outbreaks and severe convection in middle latitudes. Cyclonic TPV longevity is unique to polar regions due to the relatively limited role of latent heating and the more dominant role of longwave radiative cooling. TPVs are also important to global circulations as recent studies have shown that cyclonic TPVs can exit the Arctic and interact with the polar jet, causing the initiation of Rossby wave packets on the polar jet. Rossby wave initiation and subsequent Rossby wave breaks (RWBs) and blocking patterns cause high-impact weather from droughts and floods to heatwaves and cold air outbreaks. However, current models have low skill when forecasting RWBs and blocking patterns, especially in the sub-seasonal to the seasonal timeframe.

This study aims to determine if anticyclonic TPVs are associated with RWBs and impact the development and persistence of blocking patterns. It is hypothesized that anticyclonic TPVs form from poleward RWBs and are important potential vorticity anomalies that aid in the maintenance of blocking patterns. It is also hypothesized that examining the lifecycles and characteristics of anticyclonic TPVs can improve understanding and forecasting of RWBs and blocking patterns. ERA5 data are used to create cyclonic and anticyclonic TPV and block tracks. The characteristics and lifecycles of all three are compared. Results show that anticyclonic TPVs have significantly shorter lifetimes than their cyclonic counterparts while decreasing in maximum intensity on average throughout their lifetime. Anticyclonic TPVs have less seasonal variability than cyclonic TPVs. The maxima in anticyclonic TPV genesis locations overlap the maxima in RWB and blocking frequencies. Anticyclonic TPVs are found

to be in close spatial and temporal proximity to known blocks. Composites of multiple blocking and RWB indices show that ATPVs are most commonly associated with cyclonically sheared, poleward RWBs.

Chapter 1

Introduction

1.1 Rossby Wave Breaking

Rossby wave initiation (RWI) is an area of considerable research due to its connection to events such as Rossby wave breaks (RWBs) and blocks that have major impacts on the entire atmospheric system. Riboldi et al. (2018) listed some of the most frequent causes of RWI, which include interactions between the polar and the subtropical jet (Martius et al., 2010), the presence of mesoscale convective systems (Rodwell et al., 2013; Stensrud, 2013; Röthlisberger et al., 2016; Lillo and Parsons, 2017; Parsons et al., 2019), warm conveyor belts in forming extratropical cyclones (Madonna et al., 2014; Martínez-Alvarado et al., 2014; Röthlisberger et al., 2018) and potential vorticity (PV) anomalies on the tropopause interacting with the polar jet. Recurving tropical cyclones into the midlatitude jet during extratropical transition were also added to the causes of RWI (Riboldi et al., 2018).

After a Rossby wave is initiated, changes in the dynamic and thermodynamic environment around the jet can act to build the ridge and deepen the trough resulting in amplification of the Rossby wave (Hoskins et al., 1985). When Rossby waves become highly amplified and their phase speed exceeds the background flow, they break resulting in a RWB (Polvani and Plumb, 1992; Nakamura and Plumb, 1994; Swanson et al., 1997). RWBs cause significant mixing and transport of air masses in the troposphere, stratosphere, and between both (McIntyre and Palmer, 1983; Polvani and Plumb, 1992;

Hitchman and Huesmann, 2007; Liu and Barnes, 2015). Specifically, a poleward (equatorward) RWB can introduce high (low) potential temperature air with low (high) PV into the region north (south) of the jet (Thorncroft et al., 1993; Gabriel and Peters, 2008; Masato et al., 2012). Based on whether the RWB occurs in a cyclonically or anticyclonically sheared environment can lead to either cyclonic or anticyclonic wave breaking, respectively. Cyclonic (anticyclonic) wave breaks result in the cutoff PV or potential temperature anomaly being displaced west (east) of the longitude at which the break occurred (Thorncroft et al., 1993; Peters and Waugh, 1996).

The closed PV or potential temperature anomaly will induce a reversal of the mean poleward gradient of both variables (Hoskins et al., 1985; Appenzeller and Davies, 1992; Thorncroft et al., 1993; Peters and Waugh, 1996; Gabriel and Peters, 2008; Ndarana and Waugh, 2011). Early studies defined the occurrence of a RWB when there was a reversal of the poleward PV gradient on isentropic surfaces (Baldwin and Holton, 1988). This reversal is also frequently used to define blocking patterns, which will be examined in the next subsection. Most recent studies have identified RWBs as the overturning of PV or potential temperature on isentropic or constant PV surfaces, respectively (Abatzoglou and Magnusdottir, 2006; Barnes and Hartmann, 2012; Liu et al., 2014; Liu and Barnes, 2018).

Synoptic scale RWBs have multiple impacts on the atmospheric system. Momentum from the troposphere can be transferred vertically into the stratosphere during RWBs (Waugh and Dritschel, 1999; Lu et al., 2020), leading to changes in the stratospheric polar vortex and sudden stratospheric warmings (Polvani and Waugh, 2004; Esler and Scott, 2005; Hitchman and Huesmann, 2007). RWBs are frequently followed by atmospheric blocks in the general circulation (Rex, 1950). The impacts and predictability of blocking patterns will be examined further in the following subsection.

The climatology of RWBs has also been examined extensively, with little change in location based on the definition used for a RWB. Previous studies have found Northern Hemisphere tropospheric RWBs are most common in the regions over the North Pacific and the North Atlantic basins (Postel and Hitchman, 2001; Scott and Cammas, 2002; Abatzoglou and Magnusdottir, 2006; Bowley et al., 2019). In the summer (winter), these maxima in frequencies are centered more in the central and western (eastern) portions of the oceanic basins (Scott and Cammas, 2002; Abatzoglou and Magnusdottir, 2006). Anticyclonic wave breaking is favored in the summer when the maximum of the jet is more likely to be north of its mean annual position resulting in the RWB occurring in an anticyclonically sheared environment. Cyclonic wave breaks are favored in the winter for the opposite reason as anticyclonic breaks (Strong and Magnusdottir, 2008; Bowley et al., 2019).

1.2 Blocking

Once a Rossby wave is initiated, the resulting changes to the dynamic and thermodynamic structure of the atmosphere can have major impacts on the weather patterns from the local to hemispheric scale. One possible outcome of a jet with amplified Rossby wave packets is the development of a blocking pattern (Black et al., 2004; Elliott and Smith, 1949; Hoskins and Sardeshmukh, 1987; Rex, 1950; Kautz et al., 2022). Early blocking studies and climatologies examined the development and persistence of stationary surface high pressures (Elliott and Smith, 1949). With the widespread availability of upper air observations, most modern blocking studies have based their definitions on the persistence of upper air troughs and ridges (Fang, 2004; Masato et al., 2012; Pelly and Hoskins, 2003; Tibaldi and Molteni, 1990; Kautz et al., 2022) Despite there still being no universally accepted definition for blocking, most studies rely on the

mean balanced, atmospheric state, where geopotential height decreases when moving from the equator to the poles (Kautz et al., 2022). A reversal of the gradient indicates a weakening or reversal of the westerly background flow in the midlatitudes (Pelly and Hoskins, 2003; Tibaldi and Molteni, 1990). Some studies use a specified blocking index for a particular region that is based on the departure from the climatological 500 hPa geopotential heights such as the Greenland blocking index (GBI) (Fang, 2004).

Blocking patterns can occur following a Rossby wave break (RWB) and cause an overall slowing or stagnation of the eastward progression of weather systems in the midlatitudes (Rex, 1950; Altenhoff et al., 2008). The mechanisms for the formation and maintenance of blocking patterns are not well known. The formation of blocks can be associated with anomalous upper-tropospheric ridging and advection of lower potential vorticity air (Colucci, 1985; Sanders and Gyakum, 1980). In the presence of strong extratropical cyclones, large-scale wave breaks can aid in the formation of a blocking high (Gabriel and Peters, 2008; Masato et al., 2012). For the block to persist, processes in the block must counteract the background flow that advects weather systems along the jet. This can occur from teleconnections with the tropics (Henderson et al., 2016; Moore et al., 2010) and polar regions (Biernat et al., 2021; Cohen et al., 2014), the extratropical stratosphere (Colucci and Kelleher, 2015; Quiroz, 1986), and diabatic heating sources within the blocking high or ridge (Pfahl et al., 2015; Steinfeld et al., 2020). Potential vorticity (PV) anomalies that remain after a RWB can also interact with each other and provide the force needed to counteract the progressive background flow (Altenhoff et al., 2008).

The impact of blocking patterns on weather extremes is well documented. Blocks can cause extreme warm and cold air outbreaks (Brunner et al., 2017; Karl and Quayle,

1981; Sousa et al., 2018; Whan et al., 2016; Yao et al., 2017; Kautz et al., 2022), extreme precipitation (Bissolli et al., 2011; Houze et al., 2011), summer-time thunderstorms (Mohr et al., 2019) and blizzards (Tayanç et al., 1998; Efe et al., 2019) in the midlatitudes. They can have impacts on the weather for an entire season as well (Efe et al., 2019, 2020; Quiroz, 1984). In the Arctic, blocks also produce extreme vapor transport events that can intrude into the usually dry Arctic regions (Barrett et al., 2020).

Blocking can have major impacts on the long-term weather system evolution, which impacts sub-seasonal-to-seasonal forecasts of the Arctic and mid-latitudes. However, forecast models currently have a difficult time forecasting the large-scale blocking and RWB patterns that lead to these extreme weather events (Tibaldi and Molteni, 1990; Rodwell et al., 2013; Woollings et al., 2018). There are many reasons for the lack of skill models have when attempting to forecast the development and persistence of blocking events. Models have been shown to incorrectly represent the mean background flow (Masato et al., 2013b; Priestley et al., 2020; Tibaldi and Molteni, 1990). They also frequently lack the spatial resolution (Davini et al., 2017), parameterization (Martínez-Alvarado et al., 2016; Pithan et al., 2016), or model dynamics (Williams et al., 2018) to fully resolve the smaller-scale eddies and PV anomalies that help in the maintenance of blocking patterns.

The small eddies and PV anomalies that are important to the persistence of long blocking patterns are not well-resolved by current forecasting models, which lowers these models' skill in their sub-seasonal to seasonal prediction of blocks. Understanding the development and lifecycles of these eddies and PV anomalies could improve our understanding of how blocks survive and allow us to forecast them with higher accuracy, which will in turn improve forecasts of the wide array of extreme weather these systems are known to cause.

1.3 Tropopause Polar Vortices

One possible mechanism that can initiate Rossby Waves are PV anomalies along the tropopause (Bosart et al., 1996; Hakim, 2000; Pyle et al., 2004). The importance of PV anomalies in RWI and the effects the Rossby waves have on other features in the atmosphere was discussed in Section 1.1. PV anomalies in high latitudes behave differently than other regions due to longwave radiative cooling, higher absolute vorticity, and less vertical shear (Hakim and Canavan, 2005). Because of these differences, PV anomalies originating in the polar regions are classified as tropopause polar vortices (TPVs) (Cavallo and Hakim, 2010; Hakim and Canavan, 2005). TPVs can be long-lived PV anomalies on the tropopause (Bray and Cavallo, 2022). They are mainly generated in the polar regions but can move out of the polar regions and interact with the jet stream causing Rossby wave initiation (Cavallo and Hakim, 2012; Riboldi et al., 2018) and severe thunderstorm outbreaks (Bray et al., 2021; Pyle et al., 2004). They are also associated with cold air outbreaks in the mid-latitudes (Lillo et al., 2021). Due to their tendency to sometimes have long lifetimes, TPVs could potentially be helpful as a forecasting tool on the sub-seasonal-to-seasonal time scale (Cavallo and Hakim, 2013).

TPVs can be cyclonic or anticyclonic circulations, but most previous research has focused on cyclonic TPVs. As a result, there are large gaps in knowledge of anticyclonic TPV (ATPV) development and lifecycles. While cyclonic TPVs are positive PV anomalies on the tropopause and feature an area of lower potential temperature values on the dynamic tropopause (2PVU surface) and a dry anomaly (Cavallo and Hakim, 2010), ATPVs are negative PV anomalies with higher potential temperatures on the dynamic tropopause. Previous studies have compared positive and negative PV

anomalies on the tropopause (not limited to the polar regions), finding negative (positive) anomalies are shorter-lived (longer-lived) and tend to combine with (separate from) other negative (positive) anomalies (Hakim and Canavan, 2005). The genesis and any impacts these negative PV anomalies or ATPVs have after formation are not as well-known as TPVs.

This thesis examines the formation and lifecycles of ATPVs with the goal of connecting these usually long-lived mesoscale features to the formation and maintenance of blocking patterns. It is hypothesized that ATPVs are forming from poleward-breaking Rossby waves. It is also hypothesized that after genesis, ATPVs are associated with blocking patterns as the small-scale PV anomalies that are important to the maintenance of blocks. Starting the examination of the lifecycles and characteristics of ATPVs could possibly improve our understanding and prediction of blocking patterns.

Chapter 2 will outline the data and methods used for the analysis in this thesis. Chapter 3 will examine the current requirements imposed on PV anomalies to be considered TPVs or ATPVs and propose an adjustment for ATPVs. Chapter 4 will present and explain the important results of this research. Chapter 5 will interpret the results outlined in Chapter 4 and provide possible explanations of the results. Finally, Chapter 6 will provide a summary of the study explained in this thesis and provide possible future work to be completed.

Chapter 2

Data & Methods

2.1 Cyclonic and Anticyclonic TPV Tracks

This study involved the creation of tracks for TPVs and ATPVs using the tracking algorithm TPVTrack defined in Szapiro and Cavallo (2018) and the European Center for Medium-Range Weather Forecasts (ECMWF) ERA5 reanalysis data (Hersbach et al., 2020). The ERA5 data on the dynamic tropopause (2-PVU surface) are taken from 1979 – 2021 and are limited to a 0.5° horizontal grid and 6 hourly temporal resolution, which is fine enough to resolve the meso to synoptic scale TPVs and ATPVs being tracked. The default parameters for TPVTrack outlined in Szapiro and Cavallo (2018) were designed for the spatial and temporal resolution of ERA-Interim, which consists of data at a horizontal resolution of 79 km and temporal resolution of 6 hours (Dee et al., 2011). TPVTrack is sensitive to the resolution of the data entered into the algorithm as highlighted in Szapiro and Cavallo (2018). Based on the spatial and temporal resolution used in this study, the default parameters for TPVTrack are adjusted to produce tracks of similar quantity and length to the TPV tracks created from ERA-Interim data. These updated parameters can be found in Appendix 1.

TPVs are defined as positive PV anomalies that have a lifetime longer than 2 days and spend at least 60% of that lifetime north of 65° N latitude (Hakim and Canavan, 2005). As will be discussed in Chapter 3, negative PV anomalies tend to form and spend most of their life equatorward of positive PV anomalies. For this study, the

requirements for TPVs and ATPVs are relaxed to require a lifetime longer than 2 days, and at least 60% of that lifetime spent north of 55° N latitude. This will be discussed further in Chapter 3, along with a discussion about the size criteria used for future ATPV definitions and studies.

2.2 Block Tracks

Based on the approach defined in Masato et al. (2013a), this study also developed tracks of atmospheric blocks throughout their lifetime. The same 2-PVU 6-hourly, 0.5° resolution ERA5 data from 1979 – 2021 used for TPV and ATPV tracks were used to produce block tracks. Masato et al. (2013a) defined a two-dimensional blocking index that measures the gradient of potential temperature on the 2-PVU surface. Two integrals,

$$\overline{\theta}_i^n = \frac{2}{\Delta\phi} \int_{\phi_0}^{\phi_0+\Delta\phi/2} \theta_i \, d\phi \tag{2.1}$$

$$\overline{\theta}_i^s = \frac{2}{\Delta\phi} \int_{\phi_0-\Delta\phi/2}^{\phi_0} \theta_i \, d\phi \ , \tag{2.2}$$

are calculated at each point of longitude i that extend north and south 15° in latitude ($\Delta\phi = 30°$). A running mean of 15° in longitude is also applied to focus on synoptic–scale blocking patterns.

The blocking index is calculated for a latitude band from 30°–88°N. For the latitudes that have less than $\Delta\phi/2$ between them and the pole, the $\Delta\phi$ is reduced to $\Delta\phi = 2(90 - \phi_0)$. This latitude band expands that of Masato et al. (2013a) to include the Arctic, where ATPVs are expected to develop and travel.

Using Equations 2.1 and 2.2 calculated at each point, three different blocking indices are calculated:

$$B_i = \overline{\theta}_i^n - \overline{\theta}_i^s \tag{2.3}$$

$$DB = \overline{\theta}_{i-1} - \overline{\theta}_{i+1} \tag{2.4}$$

$$RI = \overline{\theta}_i - \theta_i^* \tag{2.5}$$

where

$$\overline{\theta}_i = \frac{\overline{\theta}_i^n + \overline{\theta}_i^s}{2} \tag{2.6}$$

and θ_i^* is the daily climatological potential temperature at each grid point i. i–1 is west of i, which is west of i+1.

The direction of break index (DB) indicates whether a block is in a cyclonically or anticyclonically sheared environment relative to the background flow. A positive (negative) DB is cyclonically (anticyclonically) sheared. The relative intensity index (RI) measures the deviation from climatology in potential temperature and indicates whether the block is a poleward or equatorward intrusion of air. A positive RI is a poleward (equatorward) intrusion. The blocking index (B) will be positive when there is an increase in potential temperature on the 2-PVU moving poleward along a line of longitude. All indices are then standardized by subtracting the mean and dividing by the standard deviation at each latitude/longitude grid point. When the blocking index is positive, the tracker will check for a block based on the following criteria:

1) If a positive maximum in B remains at time $n + 1$ within a $27^\circ \times 36^\circ$ box (in latitude-longitude) centered at the maximum on day n, the block track will continue.

2) If condition 1 is met, the B, DB, and RI values at the same point as the maximum in the B field being tracked are retained as characteristics of the track.

3) If condition 1 is no longer met at time $n + 1$, the track will end at time n.

4) The track must last for at least 5 days to be considered a block and retained for analysis.

The blocking tracks are created by using the TempestExtremes tracking algorithm for tracking maxima in a field (Ullrich et al., 2021). The parameters used for the tracking and connecting of block tracks can be seen in Appendix 1.

2.3 TPV and ATPV Characteristics Comparisons

Using the tracks that were created for TPVs and ATPVs, multiple different characteristics are then compared. The lifetimes, central potential temperature, potential temperature amplitude, and radius are chosen to represent an overview of the size, intensity, and longevity of these systems. A probability distribution function is employed to compare the range each characteristic has for each type of tropopause polar vortex. A bootstrap sampling of 1000 samples is employed to determine the 95% confidence interval for each characteristic to determine ranges where ATPVs are significantly different than TPVs. A KS-test for statistical significance is also calculated to test the statistical significance of the difference of each characteristic.

Each characteristic is then examined throughout the vortex's lifetime to compare how each type of vortex evolves relative to the time after its genesis. For each characteristic, the median and interquartile range are calculated. A characteristic of the types of vortices is considered to be significantly different if the median of the characteristic of one type lies outside of the interquartile range of the other type at a period in its lifetime.

In order to examine the longest-lived and therefore most robust vortices, the above analysis is then repeated with the 95th percentile of longest-lived vortex tracks for

each respective type of vortex. This is similar to the analysis previously completed for long-track TPVs (Bray and Cavallo, 2022).

2.4 ATPV Seasonality Examination

ATPVs are then isolated and examined separately from TPVs. Similar to the characteristic comparisons explained in the previous section, the lifetimes, maximum central potential temperature, potential temperature amplitude, and radius are all compared between ATPVs in winter (DJF) and summer (JJA). Also, similar to the previous section, probability distribution functions are employed to examine the most common values for each characteristic in each season. Bootstrap resampling of 1000 samples is used to determine the 95% confidence interval and a KS-test is calculated to determine characteristics of ATPVs that are statistically significantly different based on the season.

The lifetime evolution comparisons used in the previous section are also examined for ATPVs based on the season. As in the previous section, the median and interquartile range for each characteristic is calculated throughout the lifetime. An ATPV characteristic is considered to be significantly different based on the season if the median of one season lies outside the interquartile range of the other season during a point in the lifecycle.

2.5 ATPV Spatial Distribution

In order to examine the spatial climatology and track the spatial evolution of ATPVs, multiple track density maps are created. For each track density plot, a radius of 555 km is used to determine if a point along the track is counted to the track density at

a location. This distance is chosen to correspond to similar tropopause vortex studies and is based on the most common vortex size being tracked (Hakim and Canavan, 2005; Cavallo and Hakim, 2010). The genesis density for ATPVs is created by selecting the first point from each track and applying the track density calculation. The lysis density is also calculated in the same way, but using the last point of each track. The total track density is also calculated. All density plots are in counts of ATPVs within 555 km of a point. By comparing the genesis, total track, and lysis density plots for ATPVs, common pathways for ATPVs into and through the Arctic can be determined.

2.6 Blocking Characteristics and Distributions

The blocking tracks are then examined and compared to some of the results from Masato et al. (2013a) from which the blocking algorithm used was taken. A blocking frequency distribution is created. The frequency is calculated by making count densities from the blocking tracks to indicate counts of tracks within 1500 km of a point. The counts are then divided by the number of days in the blocking dataset, which is 15,705 (1979 – 2021), in order to find the relative frequency of a block to occur at a location. This is to compare to Figure 2 from Masato et al. (2013a).

2.7 ATPV and Blocking Connection

ATPV-centered composites of the 3 standardized blocking indices are created to determine if ATPVs are associated with blocks and in what types of blocking environments are ATPVs most common. The genesis points of all ATPV tracks are selected and a 2000 $\times$ 2000 km box is drawn with the ATPV point at the center. The box size of 2000 km is selected to capture the common scale for blocking features in the dataset

of about 1500 km in diameter. The B, DB, and RI fields in the ATPV-centered box at the time of the ATPV genesis are isolated to capture the blocking environment. An average is then taken of each index for all ATPV genesis points to calculate the average value of each index at the time of ATPV genesis surrounding the ATPV location. Bootstrap resampling of 100,000 samples is calculated for each point of the ATPV-centered composites to determine statistical significance on the blocking index fields.

Chapter 3

TPV and ATPV Definition Analysis

Tropopause polar vortices were first defined in Hakim and Canavan (2005) as closed vortices on the tropopause that last longer than 2 days and spend more than 60% of their lifetime poleward of 60° N latitude. Using the TPVTrack algorithm with the parameters outlined in Appendix 1 and ERA5 data from 1979 – 2021, TPV and ATPV tracks are created based on the definition outlined in Hakim and Canavan (2005). Before applying the TPV/ATPV restrictions to the vortices tracked, there were 1,086,926 cyclonic and 1,342,547 anticyclonic northern hemisphere tropopause vortices tracked during the 43–year period. After restricting the vortices to TPVs and ATPVs, there were 45,617 TPVs and 26,254 ATPVs tracked. The ratio of total cyclonic to anticyclonic and polar cyclonic to anticyclonic tracks is similar to that found by Hakim and Canavan (2005). The reduction to about 1% of the overall tracks is expected and matches Hakim and Canavan (2005) because most tracks are less than 2 days. That is caused by the sensitivity to small circulations that appear and disappear quickly in the high-resolution ERA-5 data.

A two-week period from January into February 2021 is chosen as a case study of the tracking algorithm to determine if the tracker captures the vortices of interest for this thesis. Figure 3.1 shows a plot of potential temperature on the 2-PVU surface with the TPV and ATPV tracks plotted on top using the 65° N latitude threshold. This includes a large poleward Rossby wave break (RWB) event that occurred over Alaska

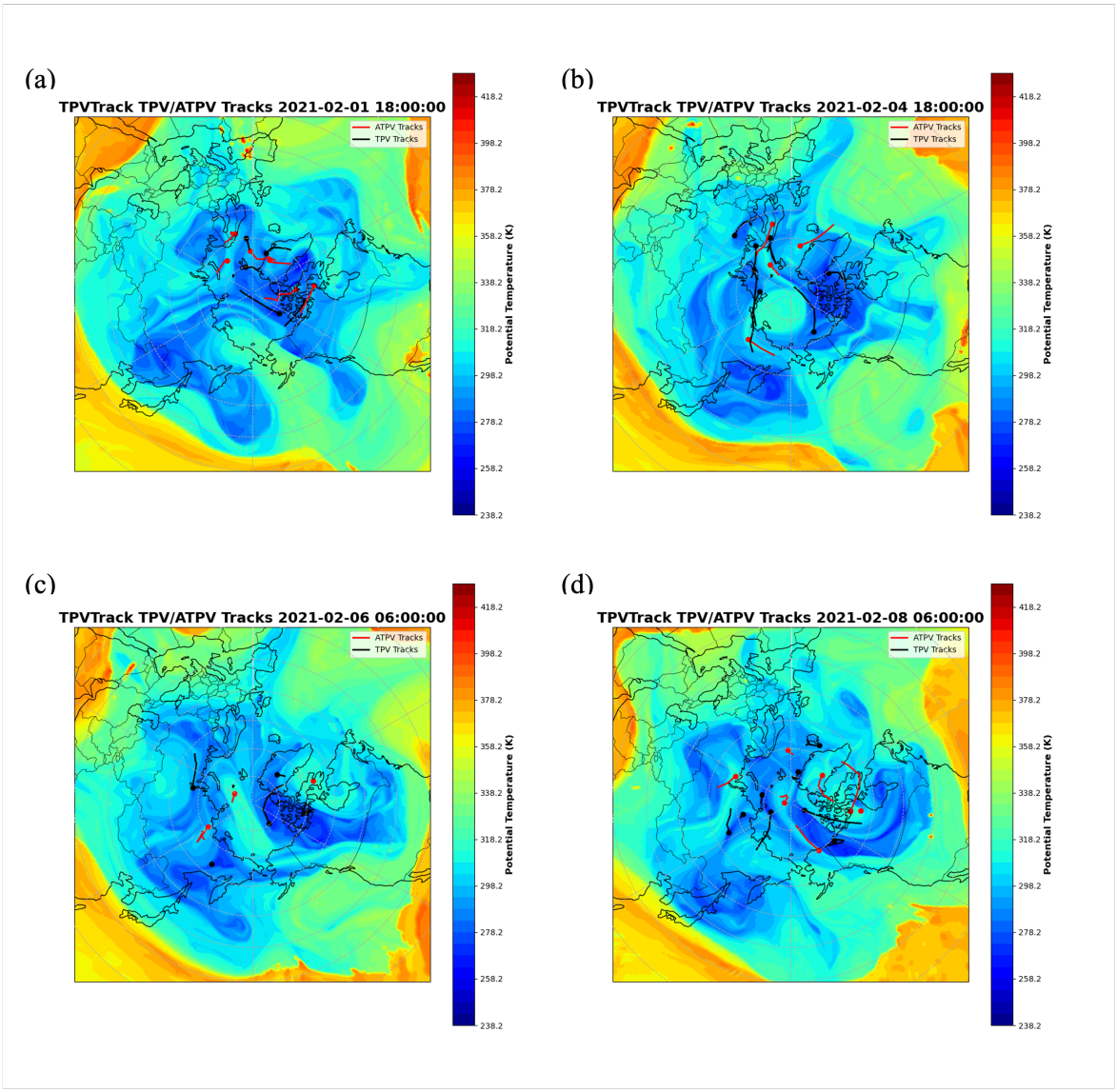

Figure 3.1: Potential temperature on the 2–PVU surface (shading) with TPV (black) and ATPV (red) tracks plotted using the 2–day minimum length and 60% of lifetime poleward of 65° N requirement. Dot represents the central point of the basin being tracked at 18z on 1 February 2021 (a), 18z on 4 February 2021 (b), 06z on 6 February 2021 (c), and 06z on 8 February 2021 (d). The tail of the track is the previous day of tracked central points of the basin.

and left a closed anticyclonic circulation north of Siberia. The Rossby wave can be seen breaking in Figure 3.1a on 1 February 2021 at 18z over Alaska and far northeastern Siberia. Three days later, on 4 February 2021 at 18z, a large area of higher potential

temperature air can be seen over the Arctic Ocean north of Siberia (Fig. 3.1b). Using the same criteria for defining TPVs to identify ATPVs leads to this significant negative PV anomaly not being considered an ATPV. That is because the negative PV anomaly is tracked out of the Arctic, where it spends more than 60% of its lifetime. For this thesis, features such as this should be considered an ATPV.

Later in the period, another RWB event occurs. The break occurs on 6 February 2021 at 06z between Greenland and the Canadian archipelago (Fig. 3.1c). In this example, the negative PV anomaly that results from the poleward RWB is tracked as an ATPV throughout its lifetime, which continues past 8 February 2021, when it is circulating around another ATPV over the Canadian archipelago (Fig. 3.1d).

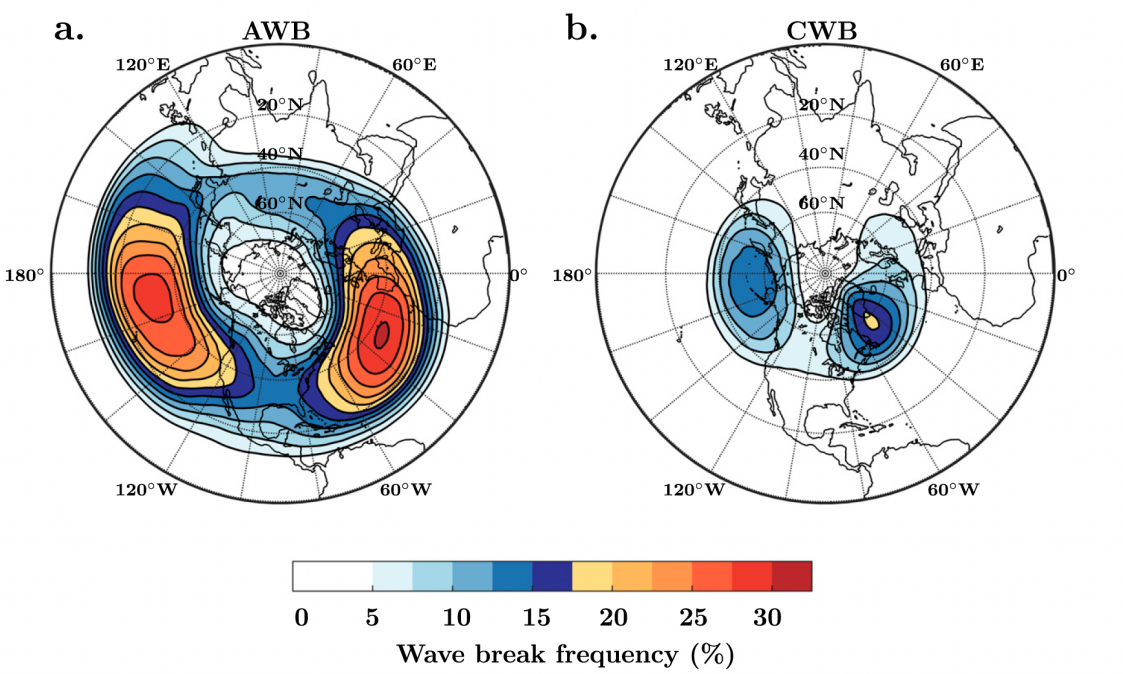

Figure 3.2: The 1979–2011 Northern Hemisphere climatological-mean (a) AWB and (b) CWB frequency. Frequency of wave breaking is contoured (black contour) every 2.5% (starting from 5%, shaded up to 30%) and denotes the percentage of time steps in the 1979–2011 period for which a grid point is classified to be in a region of instantaneous wave breaking (From Bowley et al. (2019)).

Because this thesis aims to find the connection between ATPVs and RWBs, it is necessary for ATPVs to be allowed to form near the latitudes at which RWBs most frequently occur. The most common regions for RWBs are over the North Pacific and North Atlantic (Fig. 3.2) (Bowley et al., 2019). The maxima in the frequency of both anticyclonically (AWB) and cyclonically (CWB) sheared breaks are equatorward of 60° N. CWBs are commonly poleward of AWBs and therefore are more likely to be associated with ATPV formation (Fig. 3.2b). The maxima in CWB frequency are both centered at about 55° N.

Therefore, for this thesis, the requirements for TPVs or ATPVs are relaxed to have a lifetime longer than 2 days and to spend more than 60% of that lifetime poleward of 55° N latitude. With the updated threshold the counts for TPVs and ATPVs become 61,539 and 49,894 tracks, respectively over the 43–year period. The pattern that there are fewer tropopause anticyclones than cyclones in the Arctic shown in Hakim and Canavan (2005) still holds with the modified definition. The same case study examined in Figure 3.1 is also repeated with the new definition.

At the time of the RWB over Alaska and Siberia on 1 February 2021 at 18z, the relaxed latitude definition for ATPVs allows the negative tropopause PV anomaly to be tracked as an ATPV (Fig. 3.3a). The track follows the large negative anomaly until 4 February 2021 at 18z, when the track follows a small negative PV filament that breaks away from the main circulation and travels equatorward and over central Siberia. At the same time, there are two other filaments that are tracked as ATPVs that break from the parent circulation. One passes north and east of Svalbard. The final one moves westward from far northeastern to central Siberia (Fig. 3.3b).

This case brings up another aspect of the definition of ATPVs. TPVs are usually considered to be mesoscale features that can reach the lower end of the synoptic scale

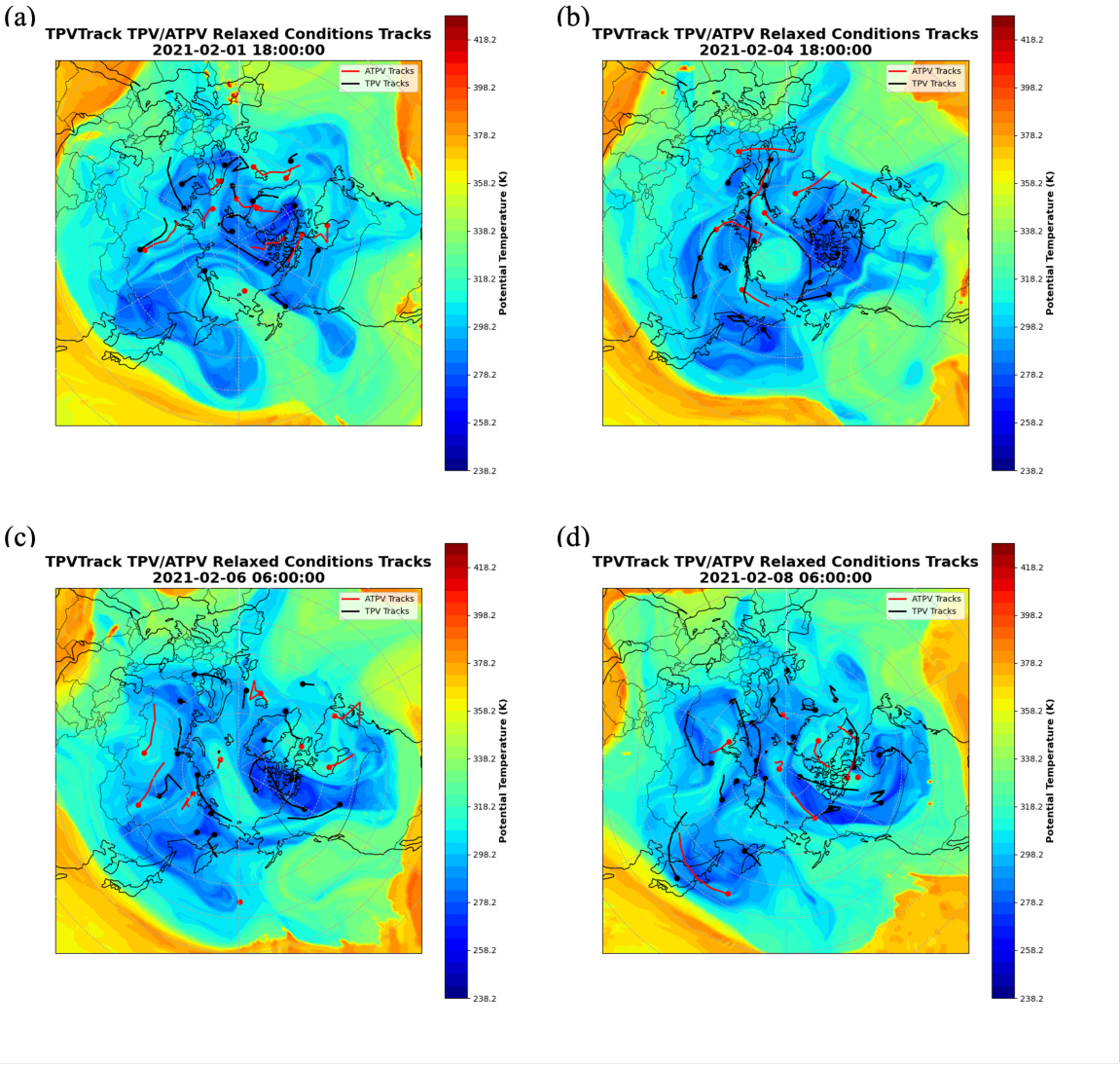

Figure 3.3: As in Fig. 3.1, but plotting the TPV and ATPV tracks using the 2–day minimum length and 60% of their lifetime poleward of 55° N requirement.

at their largest. Negative PV anomalies tend to be broader and therefore have a larger radius. They also tend to merge more frequently than positive PV anomalies on the tropopause (Hakim and Canavan, 2005). This all results in negative PV anomalies in the Arctic being larger than positive PV anomalies. The parameters for radius were held constant when tracking both positive and negative PV anomalies. As a result,

some negative PV anomalies, such as the one on 4 February 2021, are not considered to be ATPVs. That is because they are too large to be tracked as a single vortex. Rather, the tracker tracks multiple smaller vortices that rotate within the larger circulation. None of these vortices individually last longer than two days needed to meet the criteria for an ATPV. The size definition for TPVs and ATPVs will be held constant for the purposes of comparison. However, future studies on ATPVs should consider whether the large or small-scale circulations are more important to the analysis and adjust the radius definition accordingly.

The second RWB that results in a negative PV anomaly that occurs between the 6th and 8th of February 2021 between Greenland and the Canadian archipelago is still tracked as an ATPV (Fig. 3.3c, d). On 8 February 2021 at 06z, there is a TPV and an ATPV that are tracking over Japan with the 55° requirement that was not tracked using the 65° requirement (Compare Figs. 3.1d and 3.3d). This highlights the ability of the relaxed latitude requirement to track TPVs and ATPVs closer to the jet stream. The 55° N latitude requirement keeps PV anomalies that spend their entire lifetime along the jet and never enter the Arctic from being considered TPVs or ATPVs.

Some of the metrics examined in this thesis are compared using the two different latitude thresholds for ATPVs to determine their sensitivity to the requirements used. The genesis density using the 65° N requirement does not capture the strongest maximum in ATPV genesis found over Alaska using the 55° N latitude requirement (Fig. 3.4). The genesis counts of ATPVs are also lower using the 65° N requirement, which makes the genesis counts north of Svalbard of similar magnitude to the maximum over southern Greenland. When using the 55° N requirement, the maximum over southern Greenland appears more prominently. There are no significant differences between the total track and lysis densities that will be examined in Chapter 4.

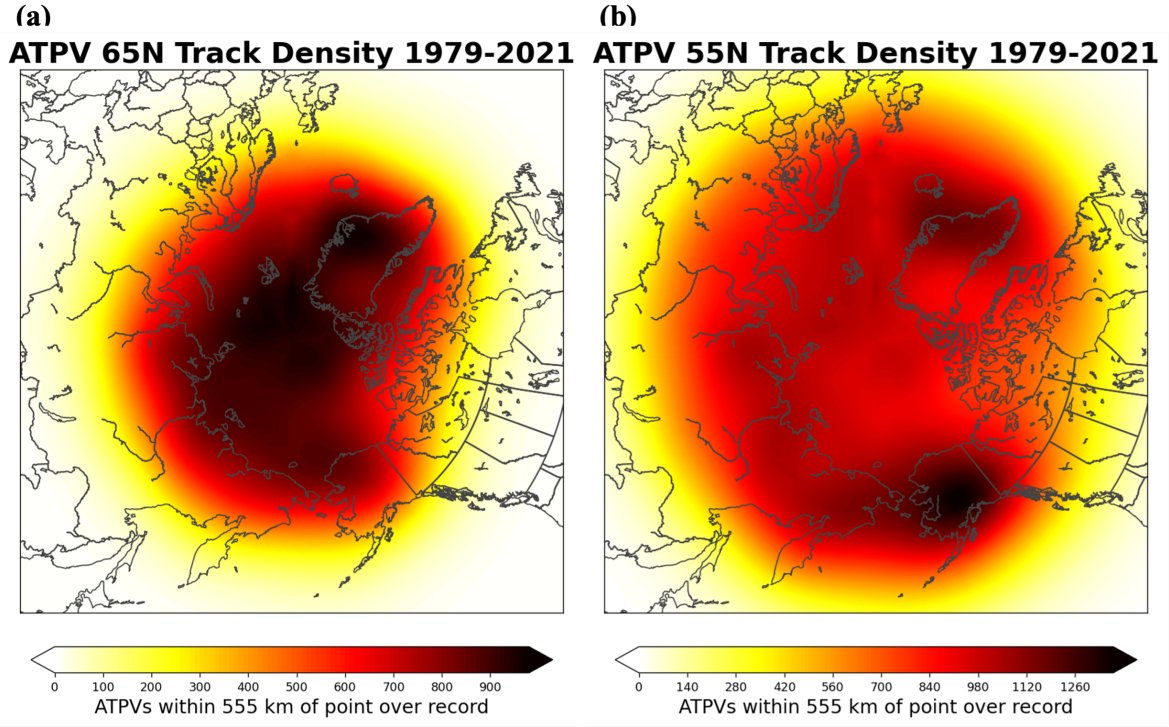

Figure 3.4: ATPV genesis density in terms of counts of ATPVs through the period from 1979 – 2021 within 555 km of a given point using the (a) 65° N and (b) 55° N latitude requirement.

The only differences in the ATPV lifetimes when comparing the two latitude requirements are in the top 99% of track lifetimes (Fig. 3.5). The longest track is about 19 days for both latitude requirements, but the probability of the longest tracks for the 55° N is lower due to the fact that there are more tracks than the 65°N requirement. The 75th and 90th lifetime percentiles are the same for both seasons of both latitude requirements at 3.75 and 5.25 days, respectively. The 95th-lifetime percentile for winter using the 65° N requirement is 6.5 days, while for winter using the 55° N requirement it is 6.25 days. The 95th-lifetime percentiles for summer using both requirements are 6.25 days. The 99th-lifetime percentiles for winter using the 65° and 55° requirements are 9.25 and 8.75 days, respectively. For summer, the 99th percentiles using the 65° and 55° requirements are 9.5 and 9.0 days, respectively.

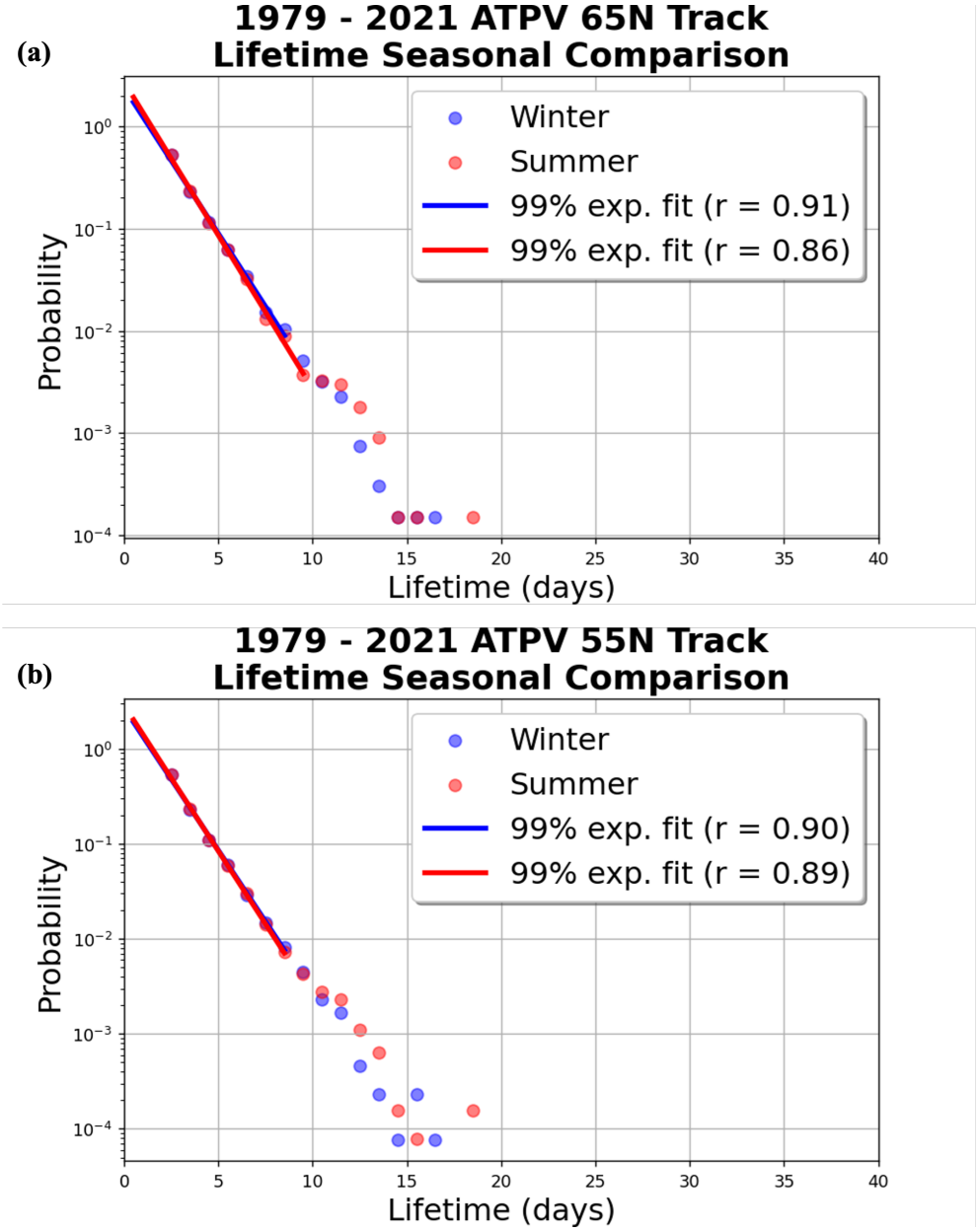

Figure 3.5: Probability distribution function of winter (blue) and summer (red) ATPV lifetimes in days using (a) 65° N and (b) 55° N requirements. Data from 1979 – 2021. The exponential best–fit line is also plotted for the bottom 99th percentile of TPV and ATPV lifetimes, with the R-values for both lines shown on the plot.

There are no significant differences between the two latitude requirements in the characteristic PDFs or characteristic lifetime evolution plots that will be shown in

Chapter 4. For the remainder of this thesis, all the plots will show only the 55° N latitude requirement for both TPVs and ATPVs.

Chapter 4

Results

4.1 TPV and ATPV Comparison

4.1.1 TPV and ATPV Lifetime Comparison

Using the updated polar definition of 55° N for PV anomalies on the tropopause, the lifetimes for both TPVs and ATPVs are analyzed.

TPVs have longer lifetimes in general than ATPVs in the Arctic (Fig. 4.1). The longest TPV track reached a lifetime of over 70 days, while the longest ATPV in the dataset was just 21 days. The lifetime percentiles for TPVs are as follows: 19.75, 11.50, 8.50, and 5.25 days for the 99th, 95th, 90th, and 75th percentiles, respectively. ATPVs have lifetime percentiles of 9.00, 6.25, 5.25, and 3.75 days for the 99th, 95th, 90th, and 75th percentiles, respectively.

A similar result was found in Figure 3 of Hakim and Canavan (2005), which showed the lifetime probabilities of all northern hemispheric tropopause vortices rather than just those in the Arctic. The slope of the exponential fit for ATPVs matches well with the slope of all anticyclonic vortices. However, the slope and maximum for TPVs are significantly different than that shown in Hakim and Canavan (2005) indicating that TPVs have longer lifetimes than all tropopause cyclonic vortices. On the other hand, ATPVs do not have significantly longer lifetimes than all anticyclonic vortices that are not limited to the Arctic.

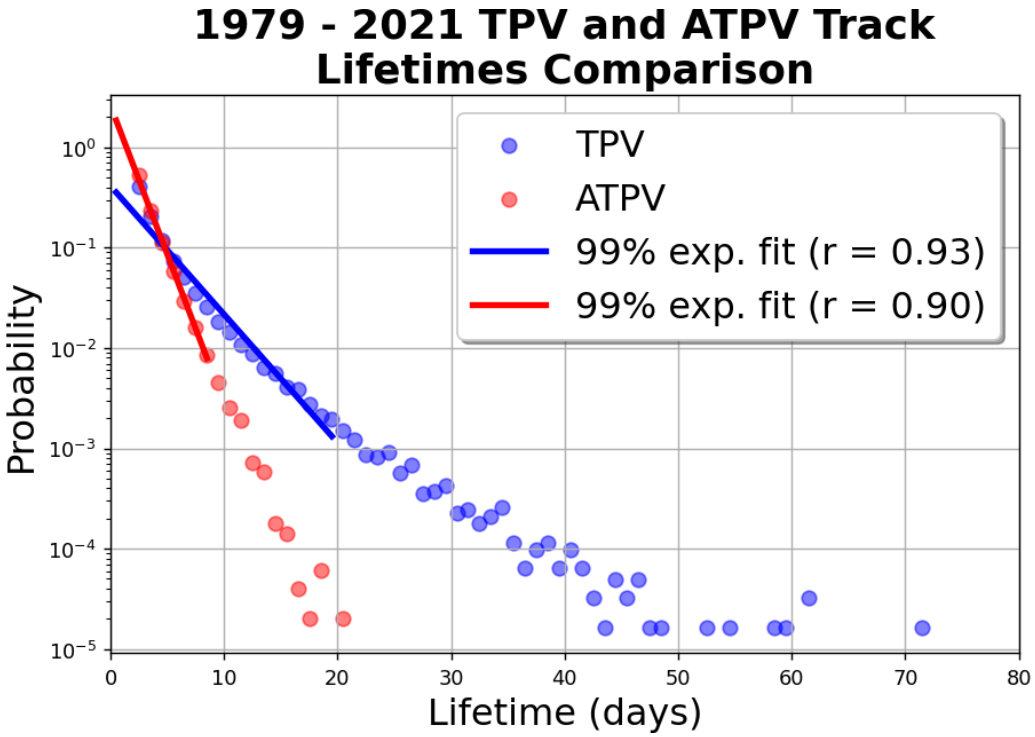

Figure 4.1: Probability distribution function of TPV (blue) and ATPV (red) lifetimes in days from 1979 – 2021. The exponential best–fit line is also plotted for the bottom 99th percentile of TPV and ATPV lifetimes, with the R-values for both lines shown on the plot.

4.1.2 TPV and ATPV Common Characteristics

The minimum potential temperature is commonly used as an indication of the intensity of TPVs; the lower the minimum potential temperature, the more intense the vortex. This can also be applied to ATPVs with the inverse being true; a higher maximum potential temperature indicates a more intense ATPV. To reduce the effect of the change in tropopause height with the season, the potential temperature amplitude is another metric used to measure the intensity of the vortex. The amplitude is calculated by subtracting the lowest potential temperature from the highest potential temperature within the circulation being tracked. For TPVs, this means the potential temperature at the center is subtracted from the maximum potential temperature along the edge of the basin being tracked. For ATPVs, the minimum potential temperature along the

edge of the basin is subtracted from the central potential temperature. To measure the size of the vortices, the radius is calculated at the equivalent radius that a circle of the same area as the basin would have.

The maximum potential temperature for ATPVs is higher than the minimum potential temperature of TPVs (Fig. 4.2a). The maximum in the central potential temperature probability for TPVs is just under 290 K, while the maximum potential temperature probability for ATPVs is about 322 K. There is also a wider distribution of ATPV potential temperatures than TPV potential temperatures, with the peak in ATPV probabilities being lower and over a larger range in potential temperatures than the peak in TPVs. There is almost no overlap in the 95% confidence intervals between the TPVs, ATPVs, and all vortices. A KS-test for significance shows that the distribution of both TPV and ATPV central potential temperatures is significantly different than all vortices with P-values of 0.000 for both to 4 significant figures.

The distributions of TPV and ATPV amplitudes are more similar than the central potential temperature (Fig. 4.2b). The most probable TPV amplitude is higher than the most probable ATPV amplitude, being about 11 K and 9 K, respectively. There is also a higher peak in the probability of ATPV than TPV amplitudes. This indicates that ATPVs tend to be weaker and have less variability in intensity than TPVs. However, there is an overlap in the 95% confidence interval over the majority of the distribution. There is no overlap between amplitudes of about 5 and 10 K, which includes the most probable ATPV amplitude. That is also the range in amplitudes that has the least overlap between each type of vortex and the all vortices distribution. A KS-test between the TPVs and all vortices indicates the distributions are significantly different with a P-value of 0.000 to 4 significant figures. The distribution of ATPV

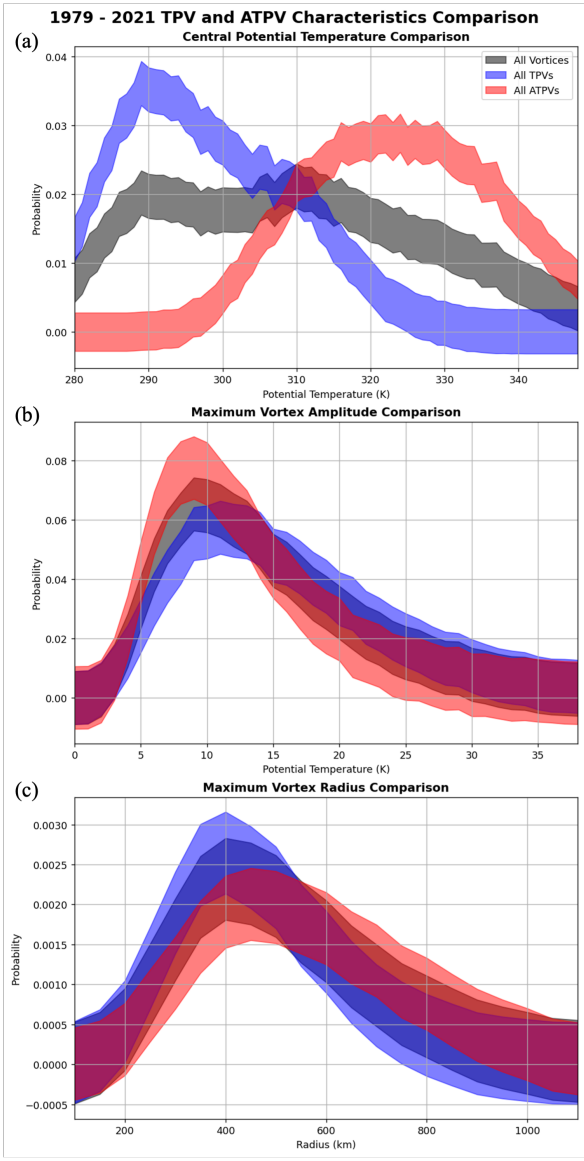

Figure 4.2: Probability distribution functions of (a) extreme (minimum for TPVs and maximum for ATPVs) central potential temperature (bin widths of 1 K), (b) maximum amplitude (bin widths of 1 K), and (c) maximum radius along the vortex tracks (bin widths of 50 km), with TPVs (blue), ATPVs (red) and all vortices (gray) all plotted. Shading represents the 95% confidence interval after a bootstrap resampling using 10000 samples is completed. KS-tests for statistically significant differences between each type of vortex and all vortices are as follows: central potential temperature – TPV: 0.000, ATPV: 0.000; amplitude – TPV: 0.000, ATPV: 0.000; radius – TPV: 0.000, ATPV: 0.000.

amplitudes is also statistically different than all vortices with a P-value of 0.000 as well to 4 significant figures.

ATPVs tend to have larger radii than TPVs, with a maximum probability at about 475 km compared to about 400 km for TPVs (Fig. 4.2c). There is less overlap in the confidence interval for the radii distribution than the amplitudes. The largest separation can be seen between 250 and 450 km, with another separation in the distributions between about 650 and 800 km. The distribution of ATPV radii also has a longer right tail than TPVs, indicating that ATPVs are more likely to grow very large. Both TPVs and ATPVs have a wide distribution in possible radii, from about 200 to close to 1000km, which makes the probability for any single radius very low. The KS-tests between the TPV and ATPV distributions and all vortices distributions are also statistically different with P-values of 0.000 to 4 significant figures as well.

4.1.3 TPV and ATPV Characteristics Throughout Their Lifetimes

The evolution of the characteristics examined in Section 4.1.2 over a vortex's lifetime leads to a better picture of how these features develop and change. In this section, the additional variable of latitude is added to depict how these vortices move latitudinally.

ATPVs tend to form at their maximum potential temperature and decrease over time (Fig. 4.3a). That can be seen on the median for ATPV potential temperature starting over 320 K at the beginning of the lifetime and ending below 320 K at the end. TPVs remain at a similar potential temperature throughout their lifetime until the final 10%, when thereafter their potential temperature increases. As expected, there is no overlap in the interquartile range of TPV and ATPV potential temperatures.

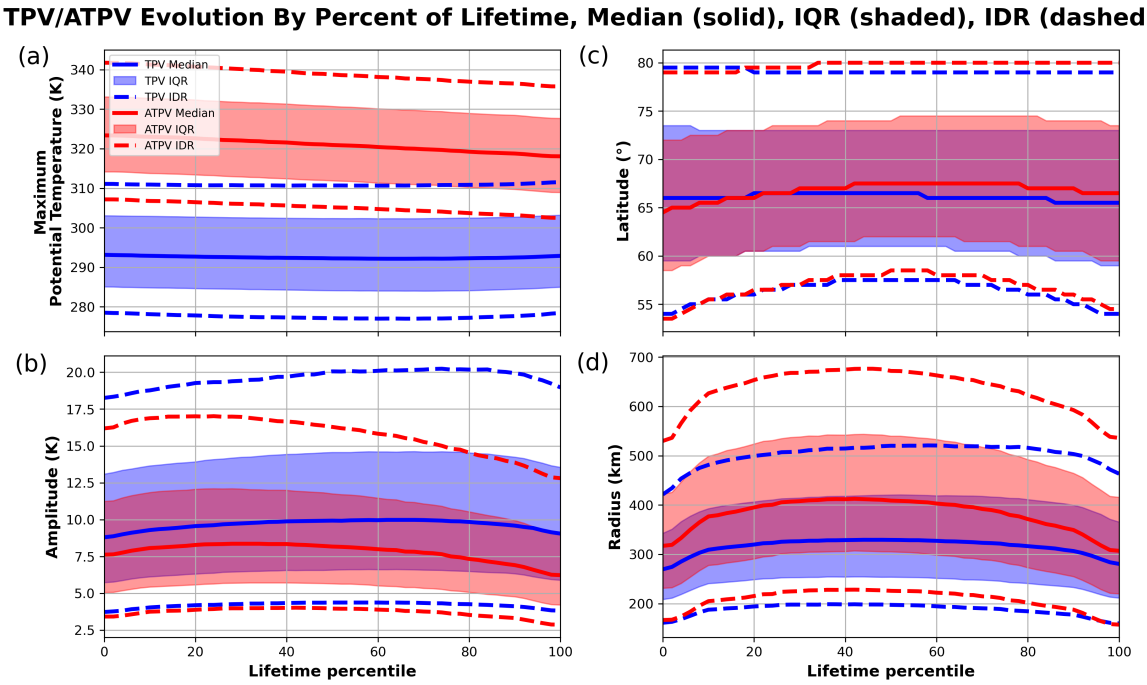

Figure 4.3: Lifetime evolution of (a) extreme (minimum for TPVs and maximum for ATPVs) potential temperature, (b) latitude, (c) amplitude, (d) radius for all TPV (blue) and ATPV (red) tracks from 1979 – 2021. Plotted in terms of lifetime percentile. The median (solid line), interquartile range (shaded region), and interdecile range (dashed lines) are also shown for each type of vortex.

When using amplitude to identify the intensity of the vortices, ATPVs do show signs of a slight increase in amplitude in the first 20% of their lifetimes (Fig. 4.3b). In contrast, TPVs show an increase in amplitude through about the first 60% of their lifetime and do not decrease in amplitude significantly until the final 10% of their lifetimes. ATPVs also have a lower amplitude than TPVs throughout their lifetime, as also seen in the results from Section 4.1.2. There is overlap in the interquartile range of TPV and ATPV amplitudes throughout their lifetimes, but the median for TPVs lies outside of the interquartile range for ATPVs at the end of their lifetimes. The upper interdecile range for TPVs is also much higher than that of ATPVs indicating that TPVs have a higher possibility for extreme amplitudes, especially near the end of their lifecycle.

The genesis latitude for ATPVs is lower than that of TPVs, but only by a few degrees (Fig. 4.3c). After genesis, ATPVs move poleward into the Arctic faster than TPVs and actually tend to reach a higher latitude than TPVs at their peak of about 67.5° N, which occurs at about the 60th percentile of their lifetime. ATPVs then move back equatorward in the last 30% of their life. The largest change in ATPV latitude with lifetime percentile overlaps with the period of increasing amplitude (Fig. 4.3b). Therefore, the period where the ATPV amplitude is increasing corresponds to them moving into an overall colder potential temperature environment rather than their maximum potential temperature increasing. TPVs are more likely to stay at the latitude at which they form, with only a slight increase in the first half of their life. The peak in TPV latitude occurs earlier than ATPVs at close to 40% of the way through their lifetime. There is a significant overlap in the interquartile and interdecile ranges for the latitude distributions of TPVs and ATPVs.

As expected based on the results from Section 4.1.2, ATPVs have a larger radius than TPVs throughout their lifetime (Fig. 4.3d). Both TPVs and ATPVs begin their lifecycle at a smaller radius and increase to a maximum radius near the midpoint of their life before decreasing in size at the end of their life. During the middle of their lifecycle, ATPVs increase in size more than TPVs, which remain more or less a constant size between the 30th and 70th percentiles of their lifetime. The maximum ATPV radius almost lies outside of the upper end of the TPVs interquartile range. More significantly, the interdecile range of ATPVs is over 150 km larger than that of TPVs for the majority of their lifetime, emphasizing the right tail toward larger radii seen in Figure 4.2c.

To compare with the results from Bray and Cavallo (2022), the TPV and ATPV tracks are limited to those in the 95th percentile for the longest tracks. The 95th

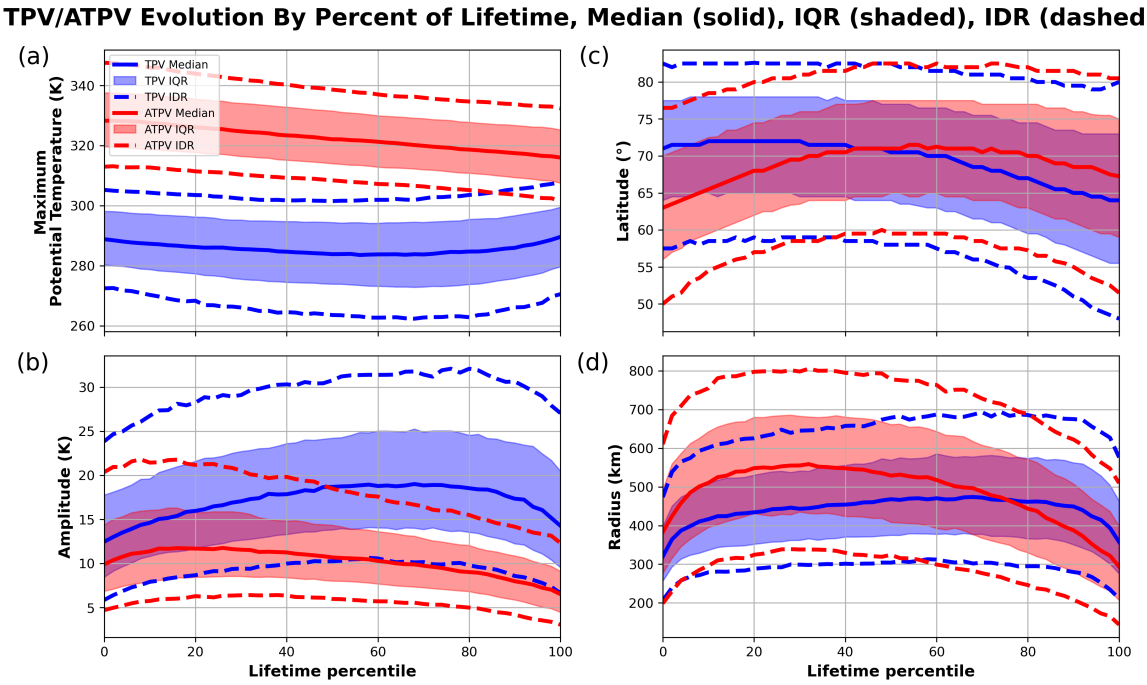

Figure 4.4: As in Fig. 4.3, but for only the 95th percentile of longest-lived TPVs (blue) and ATPVs (red).

percentiles for TPV and ATPV lifetimes are 11.5 and 6.25 days, respectively. There are 3,119 TPV and 2,756 ATPV tracks for these comparisons.

The central potential temperature for the long-track TPVs decreases to about 285 K at about the 60th percentile of their lifetime (Fig. 4.4a). That is lower and indicates a stronger vortex than all TPVs (Compare to Fig. 4.3a). The long-track ATPVs form with a higher potential temperature than all ATPVs, which also represents a stronger vortex in the case of negative PV anomalies. Both long-track TPVs and ATPVs end their lifetimes with similar central potential temperatures to all track TPVs and ATPVs.

The difference in the intensity of the long-track vortices is highlighted by the higher amplitudes of both TPVs and ATPVs (Compare Figs. 4.4b and 4.3b). The long-track TPVs reach their maximum amplitude at about the same time in their track, but they have a peak amplitude about 9 K higher than all TPVs. The amplitude difference

between long-track and all ATVPs is about 4 K. Long-track ATPVs reach their maximum amplitude earlier on in their lifetime at about the 15th percentile compared to all ATPVs which reach their maximum at about the 25th lifetime percentile.

Long-track TPVs form at a higher latitude than all TPVs (Compare Figs. 4.4c and 4.3c). On average, long-track TPVs form at about 71° N latitude, while all TPV tracks have an average genesis latitude of about 66° N. Long-track TPVs also reach farther equatorward by the end of their lifetime than all ATPVs by an average of about 3° latitude. The ATPVs that are the longest-lived form at a lower latitude than all ATPVs at close to 63° N, compared to 65° N for all ATPVs. Long-track ATPVs also reach farther poleward than all ATPVs by about 5° latitude. Both sets of ATPVs reach their most poleward extent at about the 60th-lifetime percentile.

The longest-lived TPVs have larger radii than all TPVs, reaching a maximum radius of close to 500 km (Compare Figs. 4.4d and 4.3d). Long-track TPVs reach their maximum radius close to the end of their lifetime, while all TPVs have little change in their radius throughout their lifetime. Long-track ATPVs are still larger than TPVs throughout most of their lifetime, except the final 20%. Long-track ATPVs reach a maximum radius of about 550 km, which is about 150 km larger than all ATPVs. Long-track ATPVs reach their maximum radius in the first half of their lifetime and show a considerable decrease in radius in the latter half of their lifetime.

4.2 ATPV Seasonality

4.2.1 ATPV Lifetime Seasonality

As in the previous section, the lifetimes, maximum potential temperature, amplitude, radius, and latitudes most common for ATPVs give an overview of the longevity, intensity, size, and location of these features. Another important aspect of understanding is an examination of seasonally.

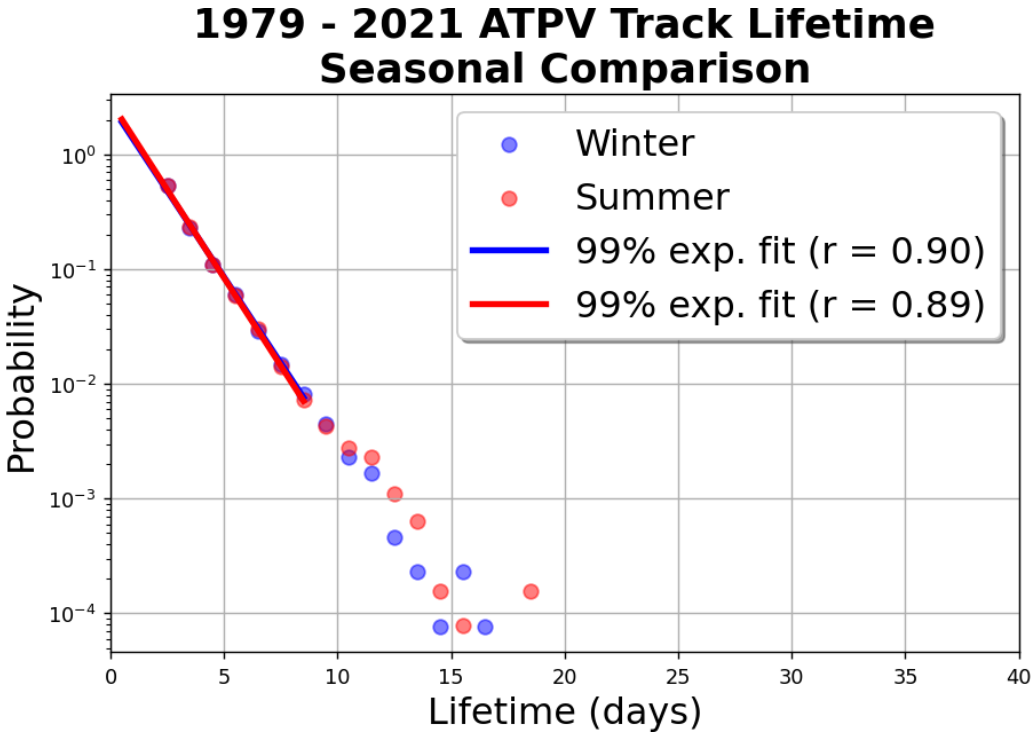

Figure 4.5: As in Fig. 4.1, but for the winter (blue) and summer (red) ATPV lifetimes.

ATPV lifetimes do not vary significantly by season (Fig. 4.5). Both winter and summer tracks have a maximum lifetime of just under 20 days. In this 43-year period being studied, the longest track between the two seasons is in the summer. It was only 2 days longer than the longest winter track. The 95th, 90th, and 75th lifetime percentiles are all the same for winter and summer at 6.25 days, 5.25 days, and 3.75

days, respectively. Only the 99th percentile is different at 8.75 days for winter and 9.00 days for winter. The best-fit lines up to the 99th percentile of track lengths for winter and summer are also almost identical.

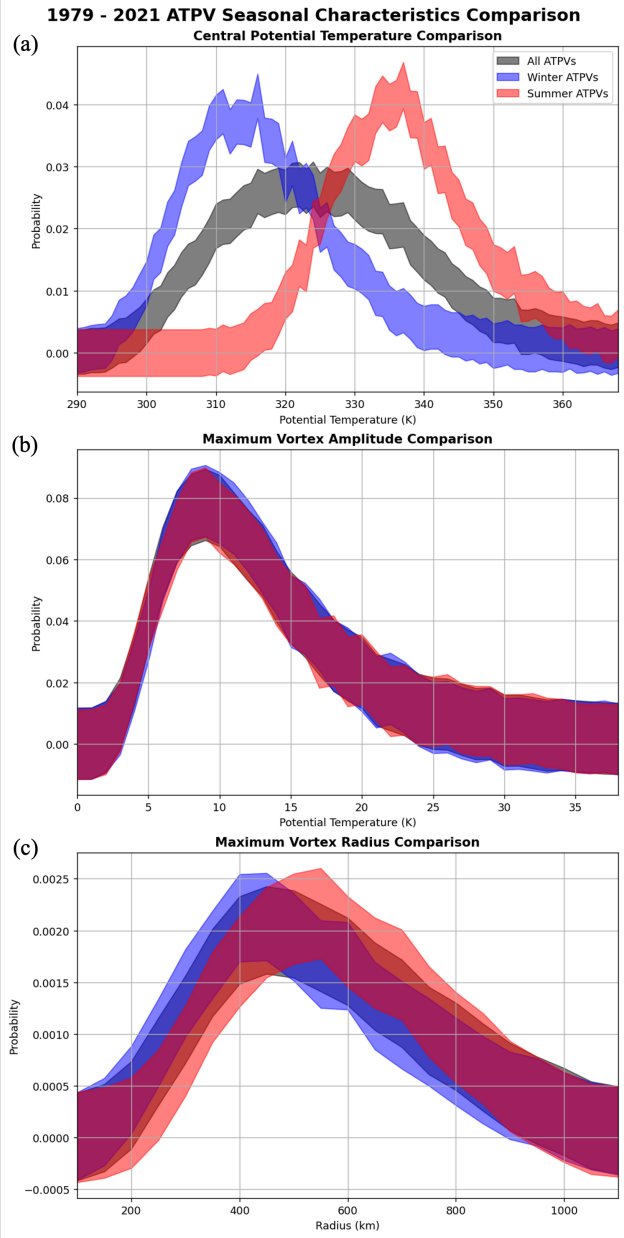

Figure 4.6: As in Fig. 4.2, but for winter ATPVs (blue), summer ATPVs (red), and all ATPVs (gray). KS-tests for statistically significant differences between each season and all ATPVs are as follows: central potential temperature – winter: 0.000, summer: 0.000; amplitude – winter: 0.319, summer: 0.460; radius – winter: 0.000, summer: 0.000.

4.2.2 ATPV Characteristic Seasonality

ATPVs show a seasonal variation in maximum potential temperature (Fig. 4.6a). In the winter their potential temperature is significantly lower than during the summer when the overall tropopause height is lower. The most probable wintertime ATPV potential temperature is about 315 K, while the maximum is about 337 K in the summer. The 95% confidence intervals of both seasonal distributions have little overlap with each other and the distribution of all ATPVs. Both distributions lack a significant tail on either side of the maximum. A KS-test indicates these distributions are all different with P-values of 0.000 for both when compared with the distribution of all ATPVs and rounded to 4 significant figures.

Similar to ATPV lifetimes, there is little variation in the radius of ATPVs based on the season (Fig. 4.6b). All three distributions have a maximum probability of about 9 K, which is the same ATPV maximum found in Section 4.1.2. There is a right tail in the distribution, showing that some ATPVs can have much higher amplitudes. However, this tail is present and almost identical in all three distributions as well. The 95% confidence intervals for both seasons completely overlap each other and the intervals for all ATPVs. This results in P-values of 0.319 and 0.460 for winter and summer, respectively, using a KS-test for significance. That means there is not a statistically significant seasonality to ATPV amplitude.

The radii of ATPVs tend to be larger in the summer than in the winter (Fig. 4.6c). The maximum probability in summertime radii is about 550 km, while the wintertime maximum is about 450 km. Both of these maxima are of similar magnitude in probability. Both distributions do have a tail to the right of their maximum in probability, showing their preference for outliers of larger radii. There is some overlap in the 95% confidence intervals, but over the majority of the distribution the winter and summer intervals are isolated from each other and the distribution of all ATPV

radii. A KS-test for statistical significance proves each season is significantly different than all ATPVs with P-values of 0.000 to 4 significant figures for both seasons.

4.2.3 ATPV Characteristic Evolution Seasonality

When examining the evolution of these characteristics over the ATPVs lifetime and separating by season, similar conclusions can be made as in Sections 4.1.3 and 4.2.2.

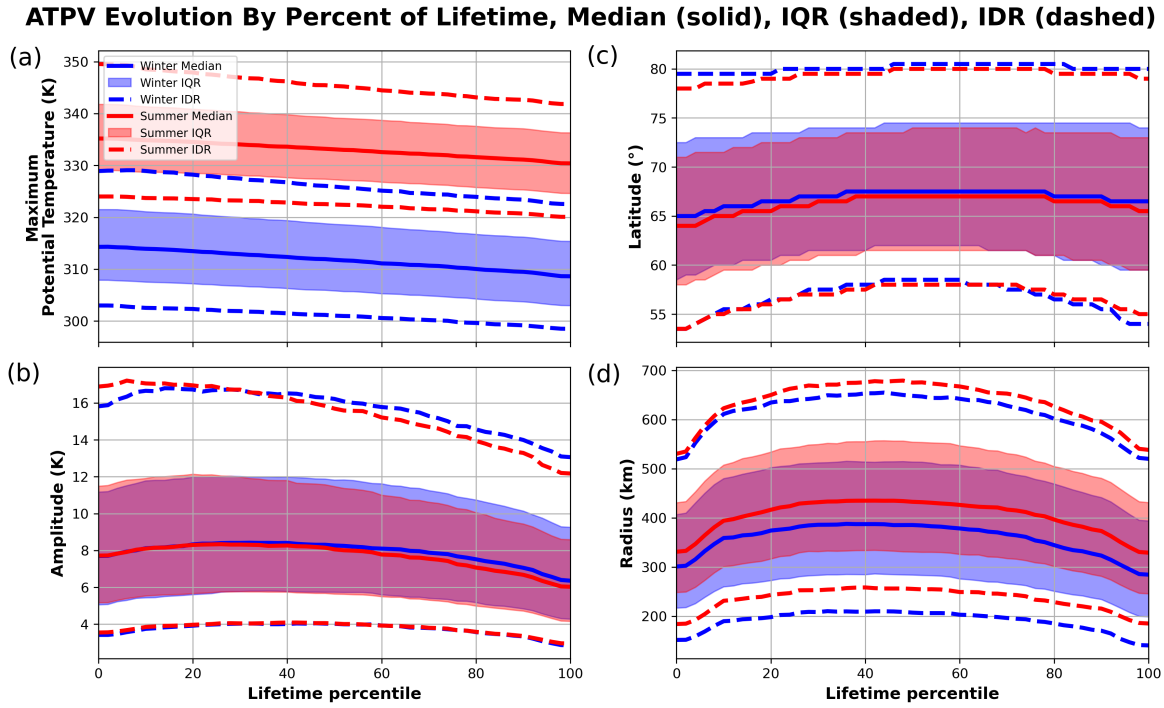

Figure 4.7: As in Fig. 4.3, but for winter (blue) and summer (red) ATPVs.

The maximum potential temperature of both winter and summer ATPVs tends to decrease throughout the ATPV lifetime (Fig. 4.7a). There is a difference in the maximum potential temperature values based on the season, but the slope of the decrease is similar. In summer, the median ATPV begins at about 335 K and decreases to about 330 K by the end of its life. In winter, the median ATPV begins at about 314 K and decreases to about 309 K at lysis. These both represent about a 5 K decrease

in potential temperature between genesis and lysis. As expected based on Figure 4.6a, there is no overlap in the interquartile range of the two seasons and even little overlap in the interdecile range throughout an ATPVs lifetime.

Unlike the maximum potential temperature, there is not a significant seasonal variation in the amplitude of ATPVs. Therefore, the lifetime evolution if both winter and summer amplitude of ATPVs matches the evolution of all ATPVs shown in Figure 4.3b. The only difference that appears is in the latter 40% of an ATPVs lifetime when winter ATPVs tend to have a higher amplitude than summer ATPVs. Outside of that, both increase in amplitude in the first 20% of their life before decreasing in amplitude for the rest of their life. They also both reach a maximum of about 8.5 K in amplitude. The final notable difference is the upper bound of the interdecile range for summer ATPVs is about 1 K higher than that of winter ATPVs.

The latitude of ATPVs throughout their lifetimes is also similar based on the season. Winter ATPVs are at a higher latitude than summer ATPVs by about 1° throughout their entire lifetime (Fig. 4.7c). Both seasons show a poleward trend in latitude over the first half of their life, with a slow equatorward trend after that. The interquartile and interdecile ranges of both seasons overlap almost completely. There is a 2° difference in the upper bounds of the interdecile ranges at the time of genesis, with wintertime being poleward of summertime.

Winter and summer ATPVs have a similar radius evolution throughout their life (Fig. 4.7d). They both start at a small radius and increase until they reach their maximum at about the 40th percentile of their life when they begin to decrease in radius size. The seasonal difference can be seen with summer ATPVs having larger radii than winter ATPVs throughout their life. Summer ATPVs tend to be 40 km larger than winter ATPVs throughout their lifetimes, with the median of summer ATPVs reaching about 430 km and the median of winter ATPVs reaching about 390

km. At no time during their lifetime does either season's median radius lie outside of the interquartile range of the other season.

4.3 ATPV Track Densities

Another important aspect of the understanding of ATPV lifecycles is the climatological genesis, track, and lysis densities. This will help with the understanding of the preferential locations for the formation of ATPVs, which can allow for further analysis of other features that have similar preferential locations for possible connections to ATPVs. By looking at the genesis and lysis locations along with the total track densities, preferred pathways for the movement of ATPVs throughout the Arctic can also be inferred.

There are two main maxima in the genesis density for ATPVs (Fig. 4.8). The strongest maximum is centered over Alaska, with a less intense area of high counts that extends across the Bering Strait and along the Arctic Ocean coast of Siberia. There is a second maximum over the southern half of the island of Greenland and east to Iceland. The connection between these locations and blocking locations will be examined in the next section. In general, there are fewer counts of genesis locations over the Arctic Ocean, but there are more over the Atlantic side of the Arctic Ocean than the Pacific side. The most noticeable area that has a local minimum in ATPV genesis counts is over Hudson Bay and the Canadian Archipelago.

The total ATPV track density has a maximum over the Arctic Ocean and the coasts of the surrounding landmasses (Fig. 4.9). Within the larger maximum, there are locally higher counts of ATPV tracks over the Beaufort Sea north of Alaska and eastern Siberia as well as between northeastern Greenland and Svalbard. The minimum

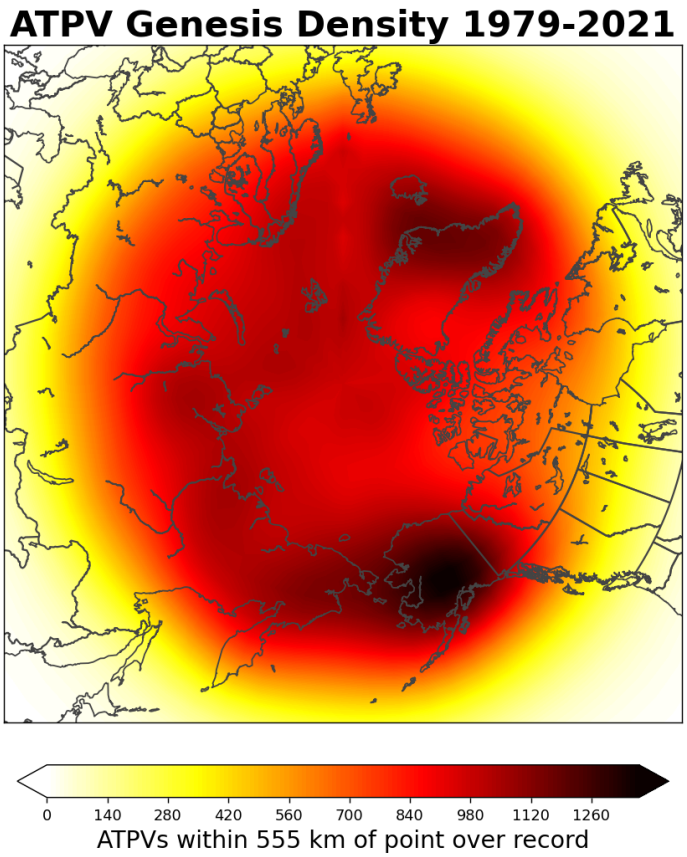

Figure 4.8: ATPV genesis density in terms of counts of ATPVs through the period from 1979 – 2021 within 555 km of a given point.

over the north pole could be an artifact of how the TPVTrack tracking algorithm tracks vortices that move near and over the pole. Another minimum in ATPV track counts is over Greenland, especially the southern half of the island, which appeared as a maximum in ATPV genesis density.

ATPV lysis locations have the highest counts over the Canadian Archipelago and extending into the northern Husdon Bay region (Fig. 4.10). A secondary maximum appears between northeastern Greenland and Svalbard, which extends north and east of Svalbard into the central Arctic. There are two maxima with lower counts along the central coast of Siberia and over the Beaufort Sea north of Alaska. The minimum

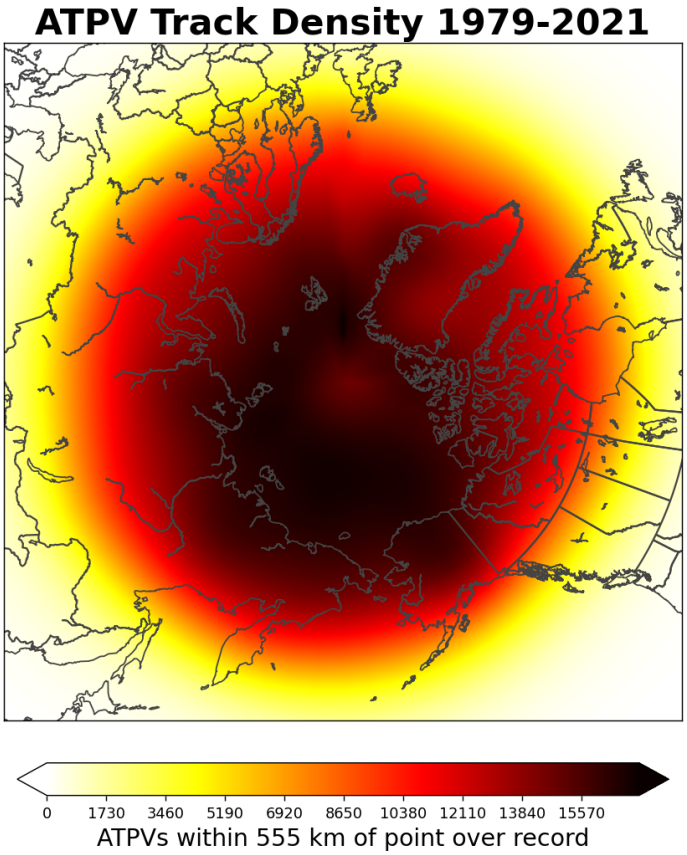

Figure 4.9: As in Fig. 4.8, but for ATPV total track point density.

in ATPV lysis density in the Arctic lies over the Pacific side of the Arctic Ocean and closer to the Siberian coast than the North American coast.

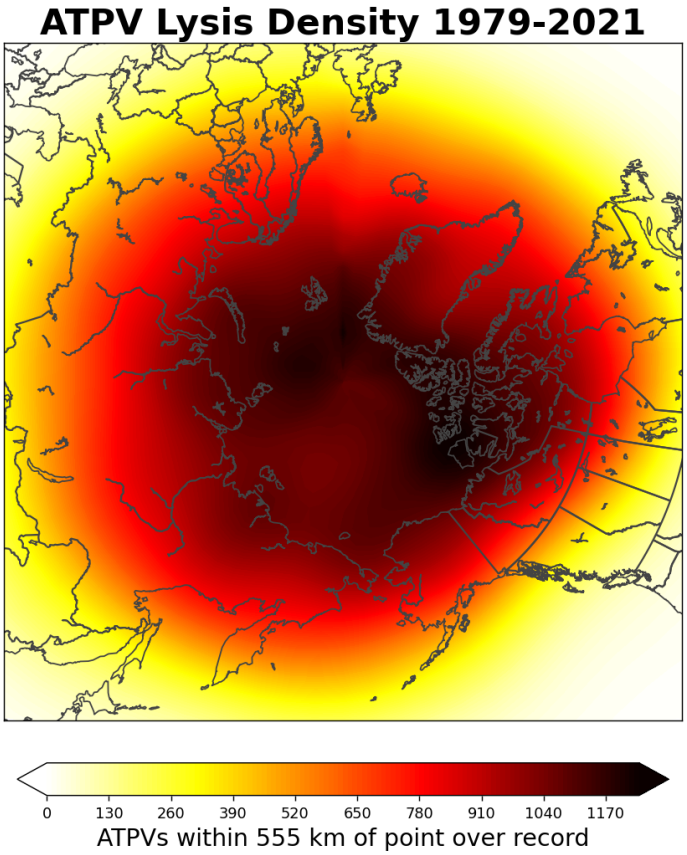

Figure 4.10: As in Fig. 4.8, but for ATPV lysis density.

4.4 Blocking Track Densities

After limiting the block tracks to only those that meet the criteria outlined in Section 2.2 about the blocks tracker, there are 839 blocks tracked throughout the period from 1979 – 2021.

There is a noticeable minimum in blocks over the Arctic that also extends equatorward over the European continent (Fig. 4.11). The maximum block track density is at the lowest latitudes tracked almost encircling the globe with the exception of over southern Europe. There are two notable extensions to the maximum along the lowest latitudes tracked. These are over the oceans adjacent to the North American continent.

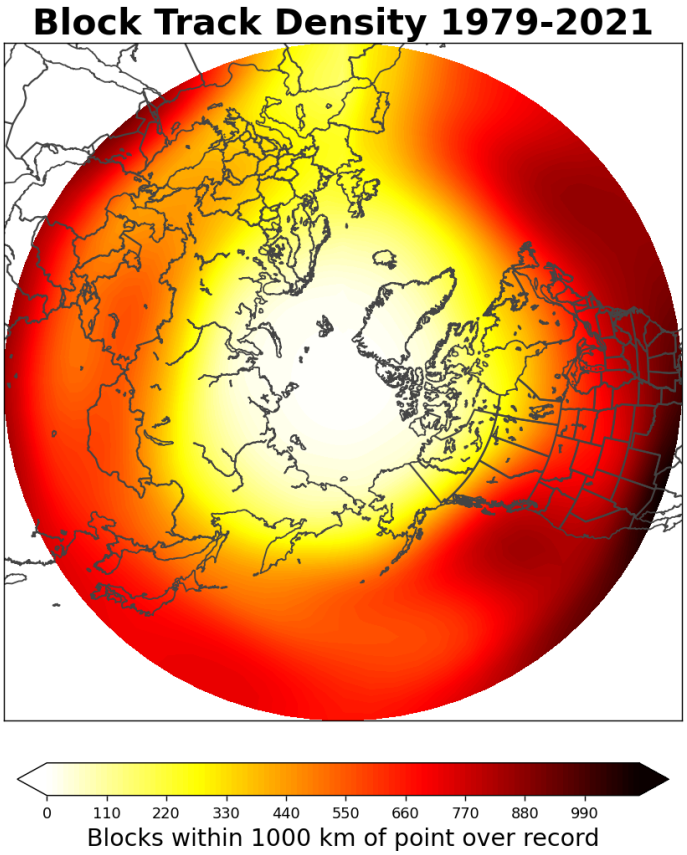

Figure 4.11: Blocks total track point density in terms of counts of blocks through the period from 1979 – 2021 within 1000 km of a given point.

The maximum over the eastern North Pacific extends poleward and also westward up to the Gulf of Alaska. The maximum over the western North Atlantic extends north and eastward over the central Atlantic and close to the southern tip of the island of Greenland.

4.5 ATPV-Centered Blocking Indices Composites

To begin the examination of ATPVs' connection to blocking patterns, composites of the three blocking indices are made for the time of ATPV genesis. These composites

will give an idea of whether blocking conditions frequently occur around ATPVs and what types of blocks with which ATPVs are most likely to be associated.

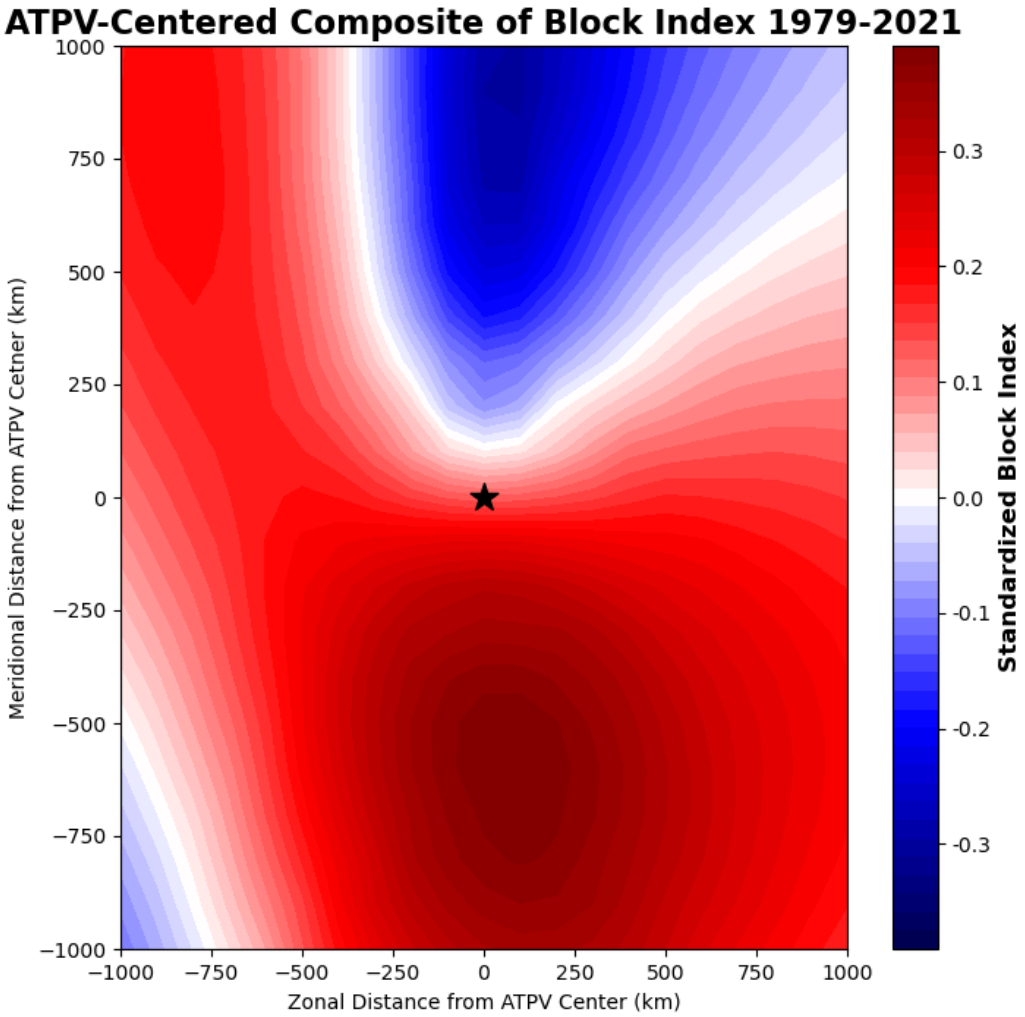

Figure 4.12: Composite of the standardized blocking index (B) at the time of the genesis of all ATPVs within the period from 1979 – 2021 extending 1000 km from the ATPV center being tracked. The star marks the location of the ATPV and the color fill is the average of the standardized blocking index surrounding all ATPV genesis points. Positive values of the blocking index indicate blocking conditions. The star represents the location of the ATPV center that was used to composite.

The composite of the blocking index centered around ATPVs at the time of genesis has a positive maximum in the blocking index about 600 km south of the ATPV center (Fig. 4.12). Positive values in the blocking index indicate there are blocking conditions. This maximum reaches an average of 0.4 standard deviations from the mean of the blocking index. There is also an area of negative blocking index about 900 km north of the ATPV center, which also reaches an average of about 0.4 standard deviations from the blocking index mean. The ATPV center itself averages a blocking index of about 0.1 standard deviations from the mean.

The ATPV-centered direction of the breaking index composite at the time of ATPV genesis has a negative maximum at about 500 km north and 250 km west of the ATPV center (Fig. 4.13). This maximum averages about 0.6 standard deviations from the mean in the direction of breaking index. A negative value in the direction of breaking index represents a cyclonically sheared environment. Positive values of the direction of breaking index represent an anticyclonically sheared environment, which appears east of the ATPV center. However, the greatest average standard deviation of the positive maximum only reaches about 0.1 standard deviations from the mean. The ATPV center lies in an average of a negative direction of breaking index that is about 0.2 standard deviations from the mean.

The ATPV center in the relative intensity index composite has an average relative intensity value of about 0.3 standard deviations from the mean (Fig. 4.14). The positive maximum in the average relative intensity index is about 250 km north and 100 km east of the ATPV center at the time of genesis. That maximum is on average just over 0.3 standard deviations from the mean relative intensity. A positive standard deviation for the relative intensity index represents a poleward intrusion of air or a poleward break.

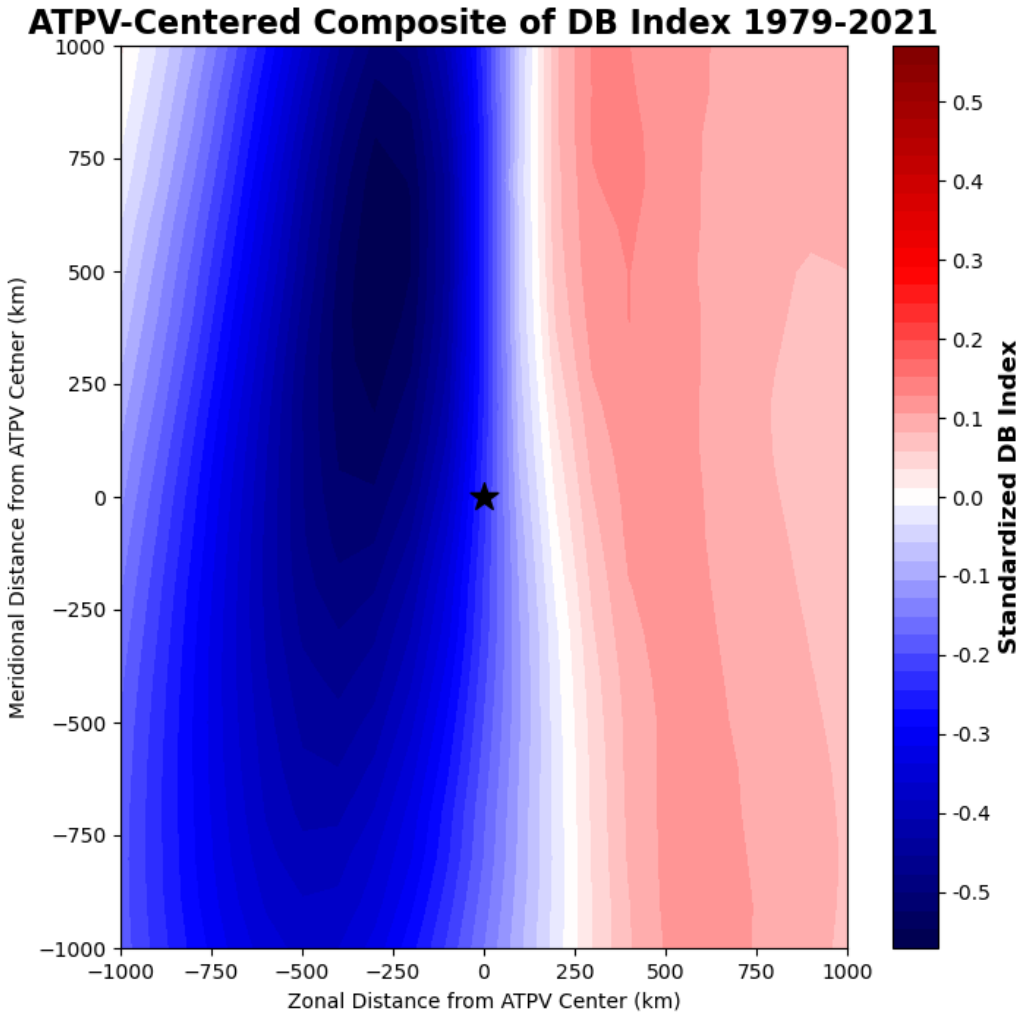

Figure 4.13: As in Fig. 4.12, but for the standardized direction of breaking (DB). Positive (negative) values of the direction of break index indicate anticyclonically (cyclonically) sheared.

There is also a maximum in negative relative intensity west of the ATPV center that reaches an average of about 0.35 standard deviations from the mean.

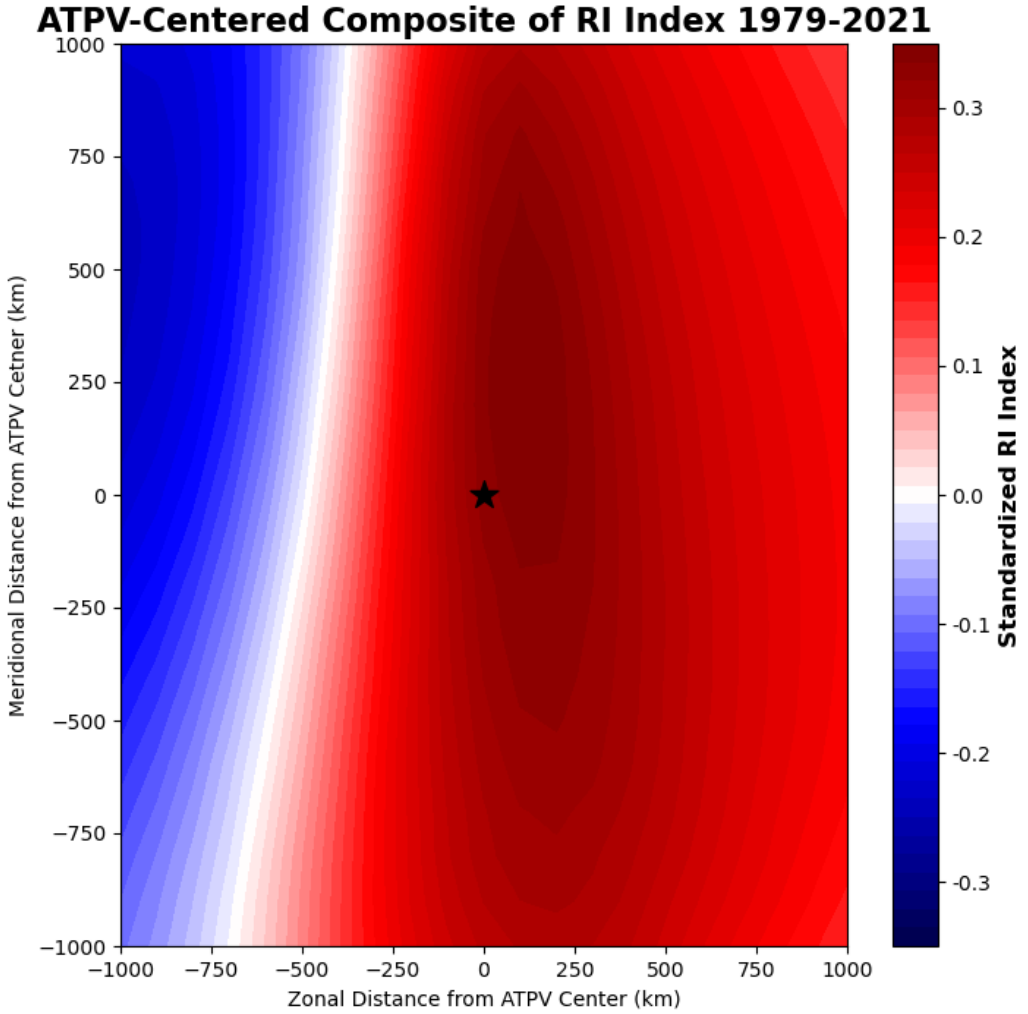

Figure 4.14: As in Fig. 4.12, but for the standardized relative intensity of breaking (RI). Positive (negative) values of the relative intensity of break index indicate poleward (equatorward) breaks.

Chapter 5

Discussion

5.1 TPV and ATPV Comparison

5.1.1 TPV and ATPV Lifetime Comparison

ATPVs are shown to have shorter lifetimes that TPVs with the longest ATPV track reaching only 21 days, while the longest TPV track reaches over 70 days (Fig. 4.1). One sustaining mechanism for TPVs longwave radiative cooling and therefore they can be maintained in the Arctic, which is dominated by longwave cooling (Cavallo and Hakim, 2013). When ATPVs form in the Arctic, there is nothing to sustain the higher potential temperatures that are present within the ATPV circulation. That leads to ATPVs having no mechanisms to maintain their local maximum potential temperature and the circulation breaks down over time. Therefore, they have a shorter lifetime on average.

When comparing the lifetime results in this thesis with those in Hakim and Canavan (2005), it can be noted that the lifetimes for ATPVs are of similar magnitude, but the lifetimes for TPVs are longer. The maximum cyclonic tropopause vortex lifetime that the study found was just under 35 days compared to the longer than 70-day maximum TPV track in this study. Hakim and Canavan (2005) analyzed the lifetimes of all PV anomalies on the tropopause, so differences in lifetimes could be from the inclusion of tracks that were not in the polar region. Positive PV anomalies outside of the Arctic

do not have the same magnitude of longwave cooling effect as those in the Arctic. Therefore, all positive tropopause PV anomalies would be expected to have shorter average lifetimes than those that spend most of their life in the Arctic. On the other hand, one possible mechanism for the maintenance of negative PV anomalies on the tropopause would be the release of latent heat. In the Arctic, there is less water vapor to condense and release substantial latent heat than at lower latitudes. Therefore, lower latitude negative tropopause PV anomalies might be expected to have longer lifetimes than those that spend most of their life in the Arctic. The fact that Hakim and Canavan (2005) found maximum negative tropopause PV anomalies over 30 days and this thesis has maximum ATPV lifetimes of just over 20 days could be a result of this difference in availability for latent heat release.

5.1.2 TPV and ATPV Common Characteristics

A significant difference in the central potential temperature within each type of tropopause circulation would be expected due to the tendency for TPVs to be a local minimum in the dynamic tropopause height and ATPVs to be a local maximum (Fig. 4.2a). The distribution of ATPV central potential temperatures is also over a wider range than TPVs. This could be from a wider seasonal variation than TPVs, which will be examined in the next section. It could also be a result of ATPVs being a product of their surrounding environment. If ATPVs form from poleward-breaking Rossby waves and have nothing to cause them to intensity after genesis, the potential temperature within the circulation will be determined by the potential temperature from which the ATPV formed. That means that for ATPVs the potential temperature within an ATPV could depend on the latitude at which it formed. TPVs do have a means for intensification in the Arctic, so it is possible that they can be intensified to a more restricted range of

central potential temperatures (Cavallo and Hakim, 2010, 2013; Hakim and Canavan, 2005).

An easier metric to compare the relative intensity of each type of vortex is the amplitude of potential temperature difference (Fig. 4.2b). The amplitude of ATPVs was also significantly different than that of TPVs. ATPVs have a smaller amplitude and less pronounced right tail toward extreme amplitude values. The conclusion that ATPVs have no mechanism in the Arctic to sustain them could explain this difference in amplitude. ATPVs also have significantly larger radii than TPVs. The combination of smaller amplitudes and larger vortex size would indicate that the potential temperature gradient from the center of an ATPV to the edge would be weaker than that of TPVs. Because the circulation around these features is proportional to the potential temperature gradient, ATPVs would also be expected to have weaker circulations.

The larger radii found with ATPVs than TPVs could be caused by the tendency for anticyclonic circulations to merge, while cyclonic circulations tend to stay separate (Fig. 4.2c) (Hakim and Canavan, 2005). In order to further justify this thought, the evolution of vortex radii will be analyzed in the following subsection. If ATPVs tend to merge with each other, there should be an increase in the vortex radius throughout its life.

5.1.3 TPV and ATPV Characteristics Throughout Their Lifetimes

The lifetime evolution of different characteristics of tropopause vortices can shed further light on the possible mechanisms that sustain and destroy these features. The central potential temperature is one significant difference between the two types of polar tropopause circulations. ATPVs start at their maximum potential temperature

and then decrease with increasing lifetime percentile (Fig. 4.3a). They also decrease at a constant rate throughout their life. This lends further evidence to the possibility that ATPVs cannot be maintained in the cold Arctic environment, so they are slowly modified by the surrounding potential temperature field, which is lower than the center of the ATPV.

TPVs tend to begin their lifetime at a higher potential temperature, which represents a weaker TPV, then show a decrease in central potential temperature or strengthening. TPVs remain close to or below their initial potential temperature until right before their lysis. This contrast with ATPVs could be another point of evidence to the fact that TPVs do have a mechanism for intensification in the Arctic while ATPVs do not.

In the previous subsection, it was noted that amplitude is a more consistent variable to use for comparing the intensity of these vortices. As expected, TPVs have a higher amplitude and show the possibility for intensification throughout their lifetimes (Fig. 4.3b). However, unlike the maximum potential temperature evolution, ATPVs do not decrease in amplitude throughout their lifetimes. They actually increase in intensity at the beginning of their life. The cause of this increase is most likely not related to an actual increase in the intensity of the vortex. Examining the definition of the amplitude can help in the understanding of this suggested intensification.

ATPVs tend to increase in latitude throughout the first 75% of their lifetime (Fig. 4.3c). Because ATPVs are a local maximum in potential temperature, the central potential temperature is warmer than the environment at the edge of the circulation. In general, traveling poleward along a line of longitude there will be a decrease in potential temperature at the tropopause. That means that if an ATPV moves to a higher latitude, the environment surrounding the circulation will decrease in potential temperature. If the ATPV moves north into the Arctic and the potential temperature at

the edge of the basin decreases faster than the central potential temperature maximum decays, that will lead to an increase in amplitude and apparent intensity. Therefore, the increase in ATPV amplitude near the beginning of its lifetime is more likely a result of its poleward movement than an indication that something is intensifying the ATPV (Compare Figs. 4.3a and 4.3b).

Because the amplitude is so closely related to the latitude and surrounding potential temperature environment, a closer look at the increase in TPV amplitude is warranted (Compare Figs. 4.3a and 4.3b). At the same time, TPVs show an increase in amplitude, they are also decreasing in latitude. For a TPV, a decrease in latitude means that it is moving into an environment with increasing contrast to its local minimum on potential temperature. Therefore, this increase in amplitude could be a result of the meridional movement of TPVs. All of this indicates that the central potential temperature is a better measurement of intensity when analyzing a vortex throughout its life and amplitude is a better measure of intensity when comparing different vortices.

The radius of ATPVs is larger than TPVs throughout their lifetimes (Fig. 4.3d). ATPVs do also show more variability in radius during their lifetime. While TPVs tend toward a constant radius except at the beginning and end of their lives, ATPVs increase in radius through the first 40% of their life before slowly decreasing. This could be due to multiple ATPVs combining together as anticyclonic circulations on the tropopause have been shown to do Hakim and Canavan (2005). It could also be a broadening of the circulation as the potential temperature maximum erodes and the anticyclonic circulation surrounding the vortex decreases. As seen in Figure 3.3b, something that was frequently observed in the latter part of an ATPVs' lifetime was the stretching of the vortex into filaments around the edges. That could be an explanation for the general decrease in radius size after the maximum is reached within the first half of an ATPV's life.

When examining only the longest-lived vortices (95th percentile for TPV and ATPV lifetimes), both long-track TPVs and ATPVs are more intense than all TPVs and ATPVs (Fig. 4.4). Long-track ATPVs still show a consistent decrease in maximum potential temperature and amplitude throughout their lifetimes. Therefore, the longest-lived ATPVs most likely last longer because they begin at a higher amplitude, so it takes a longer time for them to decay to the background environment. Long-track ATPVs also form at a lower latitude, which could mean they are breaking from a higher potential temperature region since the potential temperature on the tropopause tends to increase when moving equatorward. That would explain the higher initial central potential temperature. Long-track ATPVs also reach a higher latitude when compared to all ATPVs. They have more time to move poleward after forming than all ATPVs do. Long-track ATPVs are also larger than all other ATPVs. That could be a product of the intensity of the Rossby wave break that forms them. A larger more intense break at a lower initial latitude will lead to a longer-lived ATPV. As with all ATPVs, the longevity, and evolution of long-track ATPVs are closely related to the initial conditions with which they form.

5.2 ATPV Seasonality

5.2.1 ATPV Lifetime Seasonality

When focusing on only ATPVs and analyzing the seasonal variation there are fewer differences than in the comparison between TPVs and ATPVs. That is first evident when looking at the seasonality of ATPV lifetimes. There is little difference in the lifetimes of ATPVs in the summer and winter (Fig. 4.5). In the lower 99th percentile for ATPV lifetimes, the slope of the best-fit line is steeper than the slope for winter. That would indicate that summer ATPVs have slightly shorter lifetimes than winter

ATPVs. However, in the top 1% for longest ATPV tracks, summer ATPVs are slightly longer-lived. The longest track in the period did also occur in the summer. A possible reason for the longer summer tracks could be the higher water vapor content in the summer, which would lead to the possible increased role of latent heat release. With the differences being so small, this could also be within the margin of error.

5.2.2 ATPV Characteristic Seasonality

Similar to the comparison between TPVs and ATPVs the maximum potential temperature distributions for winter and summer are significantly different (Fig. 4.6a). Because this is a comparison between different vortices, the maximum potential temperature is not as helpful as amplitude when examining differences in intensity. The amplitude difference between winter and summer ATPVs is not statistically significant (Fig. 4.6b). Therefore, ATPVs do not show a significant difference in intensity based on the season. If ATPVs are a product of their surrounding environment, it would be expected that even as the overall environment changes based on season, there is not a change in intensity. This is further evidence of the fact that there is no maintenance mechanism for ATPVs that changes based on season and would impact the intensity of ATPVs in different seasons.

The radius of ATPVs is significantly different based on the season. Summer ATPVs are more likely to have larger radii than winter ATPVs (Fig. 4.6c). Knowing that anticyclonic PV anomalies tend to combine together could explain this seasonal difference. In the summer, the Arctic tropopause overall has higher potential temperature values. That could lead to more areas of local potential temperature maxima and negative PV. These negative PV anomalies would want to combine to form larger ATPVs. There would also be less widespread areas of lower potential temperature on

the Arctic tropopause. These lower potential temperature areas could prevent ATPVs from combining in the winter, but their absence in the summer could make the combination easier.

5.2.3 ATPV Characteristic Evolution Seasonality

Expanding the seasonal ATPV characteristic examination by season to the evolution over an ATPVs lifetime can help to understand and verify some of the ideas in the previous subsection. Both winter and summer ATPVs decrease in maximum potential temperature, and therefore intensity, throughout their lifetime (Fig. 4.7a). They also both decrease at about the same rate. That indicates that whatever is causing the decay in potential temperature is consistent through the seasons. If the decrease in ATPV intensity is solely due to the tendency for the local maximum to decrease to the state of the environment surrounding it, the similar rates of decrease between the seasons would indicate similar differences between the maximum and environment or amplitude. That is exactly what is found in the amplitude lifetime evolution. The winter and summer amplitudes are nearly identical for the first half of an ATPV's lifetime (Fig. 4.7b). The seasonal amplitude does diverge a little in the latter half of an ATPV's lifetime but by only about 0.5 K.

Both summer and winter APTVs also show a similar latitude evolution. Winter ATPVs are at a higher latitude than summer ATPVs throughout their lifetimes (Fig. 4.7c). This may not be the most obvious of results. If ATPVs are forming from Rossby wave breaks from the jet, it would be expected that they would form close to the latitude of the jet. However, the jet is at a higher (lower) latitude in the summer (winter), but ATPVs are forming more equatorward (poleward). A possible explanation for this is that Rossby wave breaks tend to be stronger in the winter than in the summer, meaning they are injected deeper into the Arctic, but further research

is needed to demonstrate that. The jet is also more amplified in the winter overall, meaning that even though the mean latitude of the jet is more equatorward in the winter, the ridges that are breaking reach similar or higher latitudes.

As examined in the previous subsection, ATPV radii are larger in the summer than in the winter (Fig. 4.7d). The radius evolution throughout an ATPV's lifetime in both winter and summer is very similar. That could lend doubt to the theory explained in the previous subsection about increased merging in the summer. It could be that summertime ATPVs just have broader circulations with fewer areas of low potential temperature to restrict them.

5.3 ATPV Track Densities

The most common regions for ATPVs to form are over the nearest landmasses poleward of the Atlantic and Pacific Ocean basins (Fig. 4.8). These regions match very well with the frequency of cyclonically sheared Rossby wave break found in Bowley et al. (2019) (Fig. 3.2b). That lends more evidence to the idea that ATPVs are forming from Rossby wave breaks. The other maxima in ATPVs genesis lie along the Arctic frontal zone across northern Siberia. This region is frequented by arctic cyclones. It is possible that these arctic cyclones are causing enough warm air advection throughout the layer to cause poleward Rossby wave breaks in the region.

After genesis, the total track density of ATPVs is centered over the entire Arctic Ocean (Fig. 4.9). There is a preference for the ATPVs to track over the Pacific side of the Arctic Ocean, but the signal is small. This indicates that there is no clear pathway for the ATPVs that form in the maximum genesis regions to move after genesis.

When continuing to the lysis density of ATPVs, there are higher maxima on the Atlantic side of the Arctic Ocean and especially over the Canadian Archipelago (Fig.

4.10). One possible reason for the maximum over the Canadian Archipelago could be from interactions with TPVs. That is the region with the highest TPV track density. When multiple TPVs interact with ATPVs, the ATPVs tend to be squeezed and stretched into filaments that are no longer tracked as ATPVs, causing the ATPV tracks to end. By examining the genesis, total track, and lysis densities, there is a possible signal for ATPVs to form north of the North Pacific and over the Siberian coast and move across the Arctic to the Atlantic side. Other than that, there is not a clear signal the ATPVs move large distances after they form.

5.4 Blocking Track Densities

If ATPVs are breaking from the polar jet and then not moving large distances after genesis, they could be connected to blocking patterns, which also frequently follow Rossby wave breaks (Rex, 1950; Altenhoff et al., 2008). In order to begin the examination of a possible connection, the track density of blocks can be examined.

Blocks are more frequent at a lower latitude than ATPVs would be tracked based on the polar definition applied (Fig. 4.11). However, there are two exceptions where the maximum block track density extends poleward closer to the polar regions. These maxima are off the west coast of North America, which extends into the Gulf of Alaska, and off the east coast of North America, which extends into the Atlantic. Both of these maxima lie just equatorward of the two maxima in ATPV genesis density discussed in the previous section. That warrants a further examination of the possible connection between ATPVs and blocks.

5.5 ATPV-Centered Blocking Indices Composites

By plotting a composite of the three blocking indices outlined in Masato et al. (2013a) centered around the ATPV track genesis locations, the most frequent type of blocking environment can be examined. To determine if there is a signal for blocks near ATPVs at the time of ATPV genesis, the blocking index (B) is composited. The composite has a bimodal pattern with a positive maximum south of the ATPV center and a negative maximum to the north (Fig. 4.12). This would be expected based on the track densities for blocks and ATPV genesis. It could also be explained by the definition of the blocking index, which measures the reversal of the poleward gradient of potential temperature on the tropopause (Masato et al., 2013a; Bowley et al., 2019; Pelly and Hoskins, 2003). An ATPV is a closed circulation with a higher potential temperature at its center. Therefore, the region south of an ATPV center would have increasing potential temperature with increasing latitude, which would show up as a block. The opposite is true for the region north of the ATPV center.

The direction of breaking index (DB) composite is divided with a signal for negative direction of breaking, or cyclonically sheared, west of and over the ATPV center (Fig. 4.13). Then, there is a region of positive, or anticyclonically sheared, direction of breaking east of the ATPV center. The fact that the ATPV is centered over the cyclonically sheared region of the block is not surprising as noted by the overlap in ATPV genesis and cyclonically sheared Rossby wave break frequency shown in Chapter 3 (Compare Figs. 4.8 and 3.2b). Because ATPVs are limited to higher latitudes, it is more likely that they will form poleward of the mean in the flow of the jet and be in a cyclonically sheared environment. Cyclonically sheared blocks have also been found to last longer than anticyclonically sheared blocks (Bowley et al., 2019). It should be noted that the direction of breaking index is used to diagnose which side of a ridge or

trough the block occurs. Because the composite ATPV center has a negative direction of breaking index means ATPVs are more likely to form on the cyclonically sheared or upstream of the ridge from which they are breaking. There are some ATPVs that form on the anticyclonically sheared side, shown by the fact that the composite ATPV center is not at the negative maximum in the direction of breaking composite.

Finally, the relative intensity index (RI) composite also behaves as expected. The ATPV is centered over a region of positive relative intensity index on average which means ATPVs are more frequently associated with poleward blocks and breaks (Fig. 4.14). That would be expected since they are an area of locally high potential temperature on the tropopause. All of these composites indicate that ATPVs could be connected with blocking patterns. If they are, they would most likely be associated with blocks that form from poleward Rossby wave breaks in cyclonically sheared environments.

It should be noted that the deviations from the mean for all three of the blocking and breaking indices are small and none of them have a statistical significance greater than 60% confidence. These are an average of almost 50,000 cases, so the fact that the signal was not completely washed out is important. For future research, the composites might need to be rotated to be aligned with the location of the block to reduce the impact the location of ATPV genesis relative to the block has on the averaging. That means these results should be a preliminary indication that there is a connection that should be explored further.

Chapter 6

Summary and Conclusions

6.1 Summary

ATPVs are closed anticyclonic circulations on the polar tropopause. They are distinct from TPVs, which are usually defined as having cyclonic circulation. This thesis aimed to develop an understanding of the formation and lifecycles of ATPVs and their possible connections to Rossby wave breaking of the polar jet stream and atmospheric blocking. To compare ATPVs to TPVs, tracks for both were created using ERA5 data from 1979 – 2021 and the TPVTrack algorithm outlined in Szapiro and Cavallo (2018). To compare ATPVs to blocks, the criteria for identifying and tracking blocks in Masato et al. (2013a) was implemented on ERA5 data from the same 1979 – 2021 period of the ATPV tracks.

This thesis found that on average ATPVs have shorter lifetimes than TPVs. They are also more likely to have a weaker amplitude when compared to the surrounding environment and a larger average radius. In contrast with TPVs, ATPVs are found to have no mechanisms for intensification after their formation. As a result, they weaken over time, while TPVs maintain their intensity or strengthen until the end of their lifecycle. Both TPVs and ATPVs tend to move poleward throughout their life, but ATPVs start at a lower latitude on average. ATPVs are then more likely to move to a higher latitude than an average TPV before they both tend to move back equatorward before their lysis.

ATPVs have some seasonal variation, especially in their maximum potential temperature and radius. They have a lower maximum potential temperature and a smaller average radius in the winter than in the summer. However, there is no significant difference in ATPV amplitude and latitude based on the season. ATPVs may form and remain at a higher latitude in the winter than in the summer, which is not the expected result. That could be explained by the possibility that wintertime Rossby wave breaks are more intense and therefore travel deeper into the Arctic than summer breaks, which may remain closer to the jet after genesis. ATPVs also do not show a significant difference in lifetime based on season, which could be further evidence that there is no process to sustain them, which means they decay at the same rate in both seasons.

The most frequent ATPV genesis locations tend to be poleward of the Atlantic and Pacific basins, which are also the most frequent regions for Rossby wave breaking. There are also poleward extensions in the maximum block frequency that approach the regions of the most frequent ATPV genesis. After genesis, there is not a strong signal for common pathways through the Arctic. There is a signal for ATPVs forming more frequently on the Pacific side of the Arctic and moving to the Atlantic side at the time of lysis. Otherwise, ATPVs do not move significantly after genesis, which lends more evidence to their connection with blocks. The most common types of blocks that ATPVs form around are cyclonically sheared poleward blocking patterns.

6.2 Future Work

Further analysis of the characteristics of ATPVs and connections to blocking patterns could shed more light on the mechanisms for the maintenance of blocks. Future studies should also consider the definition used to track ATPVs. With ATPVs being larger and forming at a lower latitude than TPVs, changes to the latitude and size thresholds used

for TPVs should be considered when applying them to ATPVs. Case studies for ATPVs that do show signs of intensification after genesis, would be helpful in determining if the release of latent heat can increase the ATPV's maximum potential temperature or what other processes could cause such an increase. ATPVs are a new field of study and all further analysis of their characteristics and evolution would be helpful in increasing the understanding of these features' connection to the overall atmospheric system.

Reference List

Abatzoglou, J. T., and G. Magnusdottir, 2006: Planetary wave breaking and nonlinear reflection: Seasonal cycle and interannual variability. *Journal of climate*, **19 (23)**, 6139–6152, https://doi.org/10.1175/JCLI3968.1.

Altenhoff, A. M., O. Martius, M. Croci-Maspoli, C. Schwierz, and H. C. Davies, 2008: Linkage of atmospheric blocks and synoptic-scale rossby waves: A climatological analysis. *Tellus A: Dynamic Meteorology and Oceanography*, **60 (5)**, 1053–1063, https://doi.org/10.1111/j.1600-0870.2008.00354.x.

Appenzeller, C., and H. Davies, 1992: Structure of stratospheric intrusions into the troposphere. *Nature*, **358 (6387)**, 570–572, https://doi.org/10.1038/358570a0.

Baldwin, M. P., and J. R. Holton, 1988: Climatology of the stratospheric polar vortex and planetary wave breaking. *Journal of Atmospheric Sciences*, **45 (7)**, 1123–1142, https://doi.org/10.1175/1520-0469(1988)045⟨1123:COTSPV⟩2.0.CO;2.

Barnes, E. A., and D. L. Hartmann, 2012: Detection of rossby wave breaking and its response to shifts of the midlatitude jet with climate change. *Journal of Geophysical Research: Atmospheres*, **117 (D9)**, https://doi.org/10.1029/2012JD017469.

Barrett, B. S., G. R. Henderson, E. McDonnell, M. Henry, and T. Mote, 2020: Extreme greenland blocking and high-latitude moisture transport. *Atmospheric Science Letters*, **21 (11)**, e1002, https://doi.org/10.1002/asl.1002.

Biernat, K. A., L. F. Bosart, and D. Keyser, 2021: A climatological analysis of the linkages between tropopause polar vortices, cold pools, and cold air outbreaks over the central and eastern united states. *Monthly Weather Review*, **149 (1)**, 189–206, https://doi.org/10.1175/MWR-D-20-0191.1.

Bissolli, P., K. Friedrich, J. Rapp, M. Ziese, and Coauthors, 2011: Flooding in eastern central europe in may 2010-reasons, evolution and climatological assessment. *Weather*, **66 (6)**, 147–153, https://doi.org/10.1002/wea.759.

Black, E., M. Blackburn, G. Harrison, B. Hoskins, J. Methven, and Coauthors, 2004: Factors contributing to the summer 2003 european heatwave. *Weather*, **59 (8)**, 217–223.

Bosart, L. F., G. J. Hakim, K. R. Tyle, M. A. Bedrick, W. E. Bracken, M. J. Dickinson, and D. M. Schultz, 1996: Large-scale antecedent conditions associated with the 12–14 march 1993 cyclone ("superstorm'93") over eastern north america. *Monthly weather review*, **124 (9)**, 1865–1891, https://doi.org/10.1175/1520-0493(1996)124⟨1865:LSACAW⟩2.0.CO;2.

Bowley, K. A., J. R. Gyakum, and E. H. Atallah, 2019: A new perspective toward cataloging northern hemisphere rossby wave breaking on the dynamic tropopause. *Monthly Weather Review*, **147 (2)**, 409–431, https://doi.org/10.1175/MWR-D-18-0131.1.

Bray, M. T., and S. M. Cavallo, 2022: Characteristics of long-track tropopause polar vortices. *Weather and Climate Dynamics*, **3 (1)**, 251–278, https://doi.org/10.5194/wcd-3-251-2022.

Bray, M. T., S. M. Cavallo, and H. B. Bluestein, 2021: Examining the relationship between tropopause polar vortices and tornado outbreaks. *Weather and Forecasting*, **36 (5)**, 1799–1814, https://doi.org/10.1175/WAF-D-21-0058.1.

Brunner, L., G. C. Hegerl, and A. K. Steiner, 2017: Connecting atmospheric blocking to european temperature extremes in spring. *Journal of Climate*, **30 (2)**, 585–594, https://doi.org/10.1175/JCLI-D-16-0518.1.

Cavallo, S. M., and G. J. Hakim, 2010: Composite structure of tropopause polar cyclones. *Monthly weather review*, **138 (10)**, 3840–3857, https://doi.org/10.1175/2010MWR3371.1.

Cavallo, S. M., and G. J. Hakim, 2012: Radiative impact on tropopause polar vortices over the arctic. *Monthly weather review*, **140 (5)**, 1683–1702, https://doi.org/10.1175/MWR-D-11-00182.1.

Cavallo, S. M., and G. J. Hakim, 2013: Physical mechanisms of tropopause polar vortex intensity change. *Journal of the atmospheric sciences*, **70 (11)**, 3359–3373, https://doi.org/10.1175/JAS-D-13-088.1.

Cohen, J., and Coauthors, 2014: Recent arctic amplification and extreme mid-latitude weather. *Nature geoscience*, **7 (9)**, 627–637, https://doi.org/10.1038/ngeo2234.

Colucci, S. J., 1985: Explosive cyclogenesis and large-scale circulation changes: Implications for atmospheric blocking. *Journal of Atmospheric Sciences*, **42 (24)**, 2701–2717, https://doi.org/10.1175/1520-0469(1985)042⟨2701:ECALSC⟩2.0.CO;2.

Colucci, S. J., and M. E. Kelleher, 2015: Diagnostic comparison of tropospheric blocking events with and without sudden stratospheric warming. *Journal of the Atmospheric Sciences*, **72 (6)**, 2227–2240, https://doi.org/10.1175/JAS-D-14-0160.1.

Davini, P., S. Corti, F. D'Andrea, G. Rivière, and J. von Hardenberg, 2017: Improved winter european atmospheric blocking frequencies in high-resolution global climate simulations. *Journal of Advances in Modeling Earth Systems*, **9 (7)**, 2615–2634, https://doi.org/10.1002/2017MS001082.

Dee, D. P., and Coauthors, 2011: The era-interim reanalysis: Configuration and performance of the data assimilation system. *Quarterly Journal of the royal meteorological society*, **137 (656)**, 553–597, https://doi.org/10.1002/qj.828.

Efe, B., A. R. Lupo, and A. Deniz, 2019: The relationship between atmospheric blocking and precipitation changes in turkey between 1977 and 2016. *Theoretical and Applied Climatology*, **138**, 1573–1590, https://doi.org/10.1007/s00704-019-02902-z.

Efe, B., I. Sezen, A. R. Lupo, and A. Deniz, 2020: The relationship between atmospheric blocking and temperature anomalies in turkey between 1977 and 2016. *International Journal of Climatology*, **40 (2)**, 1022–1037, https://doi.org/10.1002/joc.6253.

Elliott, R. D., and T. B. Smith, 1949: A study of the effects of large blocking highs on the general circulation in the northern-hemisphere westerlies. *J. Meteor.*, **6**, 67–85.

Esler, J., and R. Scott, 2005: Excitation of transient rossby waves on the stratospheric polar vortex and the barotropic sudden warming. *Journal of the atmospheric sciences*, **62 (10)**, 3661–3682, https://doi.org/10.1175/JAS3557.1.

Fang, Z.-F., 2004: Statistical relationship between the northern hemisphere sea ice and atmospheric circulation during wintertime. *Observation, Theory and Modeling of Atmospheric Variability: Selected Papers of Nanjing Institute of Meteorology Alumni in Commemoration of Professor Jijia Zhang*, World Scientific, 131–141, https://doi.org/10.1142/9789812791139_0006.

Gabriel, A., and D. Peters, 2008: A diagnostic study of different types of rossby wave breaking events in the northern extratropics. *Journal of the Meteorological Society of Japan. Ser. II*, **86 (5)**, 613–631, https://doi.org/10.2151/jmsj.86.613.

Hakim, G. J., 2000: Climatology of coherent structures on the extratropical tropopause. *Monthly weather review*, **128 (2)**, 385–406, https://doi.org/10.1175/1520-0493(2000)128⟨0385:COCSOT⟩2.0.CO;2.

Hakim, G. J., and A. K. Canavan, 2005: Observed cyclone–anticyclone tropopause vortex asymmetries. *Journal of the atmospheric sciences*, **62 (1)**, 231–240, https://doi.org/10.1175/JAS-3353.1.

Henderson, S. A., E. D. Maloney, and E. A. Barnes, 2016: The influence of the madden–julian oscillation on northern hemisphere winter blocking. *Journal of Climate*, **29 (12)**, 4597–4616, https://doi.org/10.1175/JCLI-D-15-0502.1.

Hersbach, H., and Coauthors, 2020: The era5 global reanalysis. *Quarterly Journal of the Royal Meteorological Society*, **146 (730)**, 1999–2049, https://doi.org/10.1002/qj.3803.

Hitchman, M. H., and A. S. Huesmann, 2007: A seasonal climatology of rossby wave breaking in the 320–2000-k layer. *Journal of the Atmospheric sciences*, **64 (6)**, 1922–1940, https://doi.org/10.1175/JAS3927.1.

Hoskins, B. J., M. E. McIntyre, and A. W. Robertson, 1985: On the use and significance of isentropic potential vorticity maps. *Quarterly Journal of the Royal Meteorological Society*, **111 (470)**, 877–946, https://doi.org/10.1002/qj.49711147002.

Hoskins, B. J., and P. D. Sardeshmukh, 1987: A diagnostic study of the dynamics of the northern hemisphere winter of 1985-86. *Quarterly Journal of the Royal Meteorological Society*, **113 (477)**, 759–778, https://doi.org/10.1002/qj.49711347705.

Houze, R., K. Rasmussen, S. Medina, S. Brodzik, and U. Romatschke, 2011: Anomalous atmospheric events leading to the summer 2010 floods in pakistan. *Bulletin of the American Meteorological Society*, **92 (3)**, 291–298.

Karl, T. R., and R. G. Quayle, 1981: The 1980 summer heat wave and drought in historical perspective. *Monthly Weather Review*, **109 (10)**, 2055–2073, https://doi.org/10.1175/1520-0493(1981)109⟨2055:TSHWAD⟩2.0.CO;2.

Kautz, L.-A., O. Martius, S. Pfahl, J. G. Pinto, A. M. Ramos, P. M. Sousa, and T. Woollings, 2022: Atmospheric blocking and weather extremes over the euro-atlantic sector–a review. *Weather and Climate Dynamics*, **3 (1)**, 305–336, https://doi.org/10.5194/wcd-3-305-2022.

Lillo, S. P., S. M. Cavallo, D. B. Parsons, and C. Riedel, 2021: The role of a tropopause polar vortex in the generation of the january 2019 extreme arctic outbreak. *Journal of the Atmospheric Sciences*, **78 (9)**, 2801–2821, https://doi.org/10.1175/JAS-D-20-0285.1.

Lillo, S. P., and D. B. Parsons, 2017: Investigating the dynamics of error growth in ecmwf medium-range forecast busts. *Quarterly Journal of the Royal Meteorological Society*, **143 (704)**, 1211–1226, https://doi.org/10.1002/qj.2938.

Liu, C., and E. A. Barnes, 2015: Extreme moisture transport into the arctic linked to rossby wave breaking. *Journal of Geophysical Research: Atmospheres*, **120 (9)**, 3774–3788, https://doi.org/10.1002/2014JD022796.

Liu, C., and E. A. Barnes, 2018: Quantifying isentropic mixing linked to rossby wave breaking in a modified lagrangian coordinate. *Journal of the Atmospheric Sciences*, **75 (3)**, 927–942, https://doi.org/10.1175/JAS-D-17-0204.1.

Liu, C., X. Ren, and X. Yang, 2014: Mean flow-storm track relationship and rossby wave breaking in two types of el-niño. *Advances in Atmospheric Sciences*, **31**, 197–210, https://doi.org/10.1007/s00376-013-2297-7.

Lu, H., M. H. Hitchman, L. J. Gray, J. A. Anstey, and S. M. Osprey, 2020: On the role of rossby wave breaking in the quasi-biennial modulation of the stratospheric polar vortex during boreal winter. *Quarterly Journal of the Royal Meteorological Society*, **146 (729)**, 1939–1959, https://doi.org/10.1002/qj.3775.

Madonna, E., H. Joos, O. Martius, C. Aebi, and S. Limbach, 2014: The interaction between warm conveyor belts and breaking rossby waves: a climatological perspective. *EGU General Assembly Conference Abstracts*, 5981.

Martínez-Alvarado, O., H. Joos, J. Chagnon, M. Boettcher, S. Gray, R. Plant, J. Methven, and H. Wernli, 2014: The dichotomous structure of the warm conveyor belt. *Quarterly Journal of the Royal Meteorological Society*, **140 (683)**, 1809–1824, https://doi.org/10.1002/qj.2276.

Martínez-Alvarado, O., E. Madonna, S. L. Gray, and H. Joos, 2016: A route to systematic error in forecasts of rossby waves. *Quarterly Journal of the Royal Meteorological Society*, **142 (694)**, 196–210, https://doi.org/10.1002/qj.2645.

Martius, O., C. Schwierz, and H. Davies, 2010: Tropopause-level waveguides. *Journal of the atmospheric sciences*, **67 (3)**, 866–879, https://doi.org/10.1175/2009JAS2995.1.

Masato, G., B. Hoskins, and T. J. Woollings, 2012: Wave-breaking characteristics of midlatitude blocking. *Quarterly Journal of the Royal Meteorological Society*, **138 (666)**, 1285–1296, https://doi.org/10.1002/qj.990.

Masato, G., B. J. Hoskins, and T. Woollings, 2013a: Wave-breaking characteristics of northern hemisphere winter blocking: A two-dimensional approach. *Journal of climate*, **26 (13)**, 4535–4549, https://doi.org/10.1175/JCLI-D-12-00240.1.

Masato, G., B. J. Hoskins, and T. Woollings, 2013b: Winter and summer northern hemisphere blocking in cmip5 models. *Journal of Climate*, **26 (18)**, 7044–7059, https://doi.org/10.1175/JCLI-D-12-00466.1.

McIntyre, M. E., and T. Palmer, 1983: Breaking planetary waves in the stratosphere. *Nature*, **305 (5935)**, 593–600, https://doi.org/10.1038/305593a0.

Mohr, S., J. Wandel, S. Lenggenhager, and O. Martius, 2019: Relationship between atmospheric blocking and warm-season thunderstorms over western and central europe. *Quarterly Journal of the Royal Meteorological Society*, **145 (724)**, 3040–3056, https://doi.org/10.1002/qj.3603.

Moore, R. W., O. Martius, and T. Spengler, 2010: The modulation of the subtropical and extratropical atmosphere in the pacific basin in response to the madden–julian oscillation. *Monthly Weather Review*, **138 (7)**, 2761–2779, https://doi.org/10.1175/2010MWR3194.1.

Nakamura, M., and R. A. Plumb, 1994: The effects of flow asymmetry on the direction of rossby wave breaking. *Journal of Atmospheric Sciences*, **51 (14)**, 2031–2045, https://doi.org/10.1175/1520-0469(1994)051⟨2031:TEOFAO⟩2.0.CO;2.

Ndarana, T., and D. W. Waugh, 2011: A climatology of rossby wave breaking on the southern hemisphere tropopause. *Journal of the Atmospheric Sciences*, **68 (4)**, 798–811, https://doi.org/10.1175/2010JAS3460.1.

Parsons, D. B., S. P. Lillo, C. P. Rattray, P. Bechtold, M. J. Rodwell, and C. M. Bruce, 2019: The role of continental mesoscale convective systems in forecast busts within global weather prediction systems. *Atmosphere*, **10 (11)**, 681, https://doi.org/10.3390/atmos10110681.

Pelly, J. L., and B. J. Hoskins, 2003: A new perspective on blocking. *Journal of the atmospheric sciences*, **60 (5)**, 743–755, https://doi.org/10.1175/1520-0469(2003)060⟨0743:ANPOB⟩2.0.CO;2.

Peters, D., and D. W. Waugh, 1996: Influence of barotropic shear on the poleward advection of upper-tropospheric air. *Journal of Atmospheric Sciences*, **53 (21)**, 3013–3031, https://doi.org/10.1175/1520-0469(1996)053⟨3013:IOBSOT⟩2.0.CO;2.

Pfahl, S., C. Schwierz, M. Croci-Maspoli, C. M. Grams, and H. Wernli, 2015: Importance of latent heat release in ascending air streams for atmospheric blocking. *Nature Geoscience*, **8 (8)**, 610–614, https://doi.org/10.1038/ngeo2487.

Pithan, F., T. G. Shepherd, G. Zappa, and I. Sandu, 2016: Climate model biases in jet streams, blocking and storm tracks resulting from missing orographic drag. *Geophysical Research Letters*, **43 (13)**, 7231–7240, https://doi.org/10.1002/2016GL069551.

Polvani, L. M., and R. A. Plumb, 1992: Rossby wave breaking, microbreaking, filamentation, and secondary vortex formation: The dynamics of a perturbed vortex. *Journal of Atmospheric Sciences*, **49 (6)**, 462–476, https://doi.org/10.1175/1520-0469(1992)049⟨0462:RWBMFA⟩2.0.CO;2.

Polvani, L. M., and D. W. Waugh, 2004: Upward wave activity flux as a precursor to extreme stratospheric events and subsequent anomalous surface weather regimes. *Journal of climate*, **17 (18)**, 3548–3554, https://doi.org/10.1175/1520-0442(2004)017⟨3548:UWAFAA⟩2.0.CO;2.

Postel, G. A., and M. H. Hitchman, 2001: A case study of rossby wave breaking along the subtropical tropopause. *Monthly weather review*, **129 (10)**, 2555–2569, https://doi.org/10.1175/1520-0493(2001)129⟨2555:ACSORW⟩2.0.CO;2.

Priestley, M. D. K., D. Ackerley, J. L. Catto, K. I. Hodges, R. E. McDonald, and R. W. Lee, 2020: An overview of the extratropical storm tracks in cmip6 historical simulations. *Journal of Climate*, **33 (15)**, 6315–6343, https://doi.org/10.1175/JCLI-D-19-0928.1.

Pyle, M. E., D. Keyser, and L. F. Bosart, 2004: A diagnostic study of jet streaks: Kinematic signatures and relationship to coherent tropopause disturbances. *Monthly weather review*, **132 (1)**, 297–319, https://doi.org/10.1175/1520-0493(2004)132⟨0297:ADSOJS⟩2.0.CO;2.

Quiroz, R. S., 1984: The climate of the 1983–84 winter—a season of strong blocking and severe cold in north america. *Monthly Weather Review*, **112 (9)**, 1894–1912, https://doi.org/10.1175/1520-0493(1984)112⟨1894:TCOTWS⟩2.0.CO;2.

Quiroz, R. S., 1986: The association of stratospheric warmings with tropospheric blocking. *Journal of Geophysical Research: Atmospheres*, **91 (D4)**, 5277–5285, https://doi.org/10.1029/JD091iD04p05277.

Rex, D. F., 1950: Blocking action in the middle troposphere and its effect upon regional climate. *Tellus*, **2 (4)**, 275–301, https://doi.org/10.3402/tellusa.v2i3.8546.

Riboldi, J., M. Röthlisberger, and C. M. Grams, 2018: Rossby wave initiation by recurving tropical cyclones in the western north pacific. *Monthly Weather Review*, **146 (5)**, 1283–1301, https://doi.org/10.1175/MWR-D-17-0219.1.

Rodwell, M. J., and Coauthors, 2013: Characteristics of occasional poor medium-range weather forecasts for europe. *Bulletin of the American Meteorological Society*, **94 (9)**, 1393–1405, https://doi.org/10.1175/BAMS-D-12-00099.1.

Röthlisberger, M., O. Martius, and H. Wernli, 2016: An algorithm for identifying the initiation of synoptic-scale rossby waves on potential vorticity waveguides. *Quarterly Journal of the Royal Meteorological Society*, **142 (695)**, 889–900, https://doi.org/10.1002/qj.2690.

Röthlisberger, M., O. Martius, and H. Wernli, 2018: Northern hemisphere rossby wave initiation events on the extratropical jet—a climatological analysis. *Journal of Climate*, **31 (2)**, 743–760, https://doi.org/10.1175/JCLI-D-17-0346.1.

Sanders, F., and J. R. Gyakum, 1980: Synoptic-dynamic climatology of the "bomb". *Monthly Weather Review*, **108 (10)**, 1589–1606, https://doi.org/10.1175/1520-0493(1980)108⟨1589:SDCOT⟩2.0.CO;2.

Scott, R., and J. Cammas, 2002: Wave breaking and mixing at the subtropical tropopause. *Journal of the atmospheric sciences*, **59 (15)**, 2347–2361, https://doi.org/10.1175/1520-0469(2002)059⟨2347:WBAMAT⟩2.0.CO;2.

Sousa, P. M., R. M. Trigo, D. Barriopedro, P. M. Soares, and J. A. Santos, 2018: European temperature responses to blocking and ridge regional patterns. *Climate Dynamics*, **50**, 457–477, https://doi.org/10.1007/s00382-017-3620-2.

Steinfeld, D., M. Boettcher, R. Forbes, and S. Pfahl, 2020: The sensitivity of atmospheric blocking to upstream latent heating–numerical experiments. *Weather and Climate Dynamics*, **1 (2)**, 405–426, https://doi.org/10.5194/wcd-1-405-2020.

Stensrud, D. J., 2013: Upscale effects of deep convection during the north american monsoon. *Journal of the atmospheric sciences*, **70 (9)**, 2681–2695, https://doi.org/10.1175/JAS-D-13-063.1.

Strong, C., and G. Magnusdottir, 2008: Tropospheric rossby wave breaking and the nao/nam. *Journal of the atmospheric sciences*, **65 (9)**, 2861–2876, https://doi.org/10.1175/2008JAS2632.1.

Swanson, K. L., P. J. Kushner, and I. M. Held, 1997: Dynamics of barotropic storm tracks. *Journal of the atmospheric sciences*, **54 (7)**, 791–810, https://doi.org/10.1175/1520-0469(1997)054⟨0791:DOBST⟩2.0.CO;2.

Szapiro, N., and S. Cavallo, 2018: Tpvtrack v1. 0: A watershed segmentation and overlap correspondence method for tracking tropopause polar vortices. *Geoscientific Model Development*, **11 (12)**, 5173–5187, https://doi.org/10.5194/gmd-11-5173-2018.

Tayanç, M., M. Karaca, and H. N. Dalfes, 1998: March 1987 cyclone (blizzard) over the eastern mediterranean and balkan region associated with blocking. *Monthly weather review*, **126 (11)**, 3036–3047, https://doi.org/10.1175/1520-0493(1998)126⟨3036:MCBOTE⟩2.0.CO;2.

Thorncroft, C., B. Hoskins, and M. McIntyre, 1993: Two paradigms of baroclinic-wave life-cycle behaviour. *Quarterly Journal of the Royal Meteorological Society*, **119 (509)**, 17–55, https://doi.org/10.1002/qj.49711950903.

Tibaldi, S., and F. Molteni, 1990: On the operational predictability of blocking. *Tellus A*, **42 (3)**, 343–365, https://doi.org/10.1034/j.1600-0870.1990.t01-2-00003.x.

Ullrich, P. A., C. M. Zarzycki, E. E. McClenny, M. C. Pinheiro, A. M. Stansfield, and K. A. Reed, 2021: Tempestextremes v2. 1: a community framework for feature detection, tracking, and analysis in large datasets. *Geoscientific Model Development*, **14 (8)**, 5023–5048, https://doi.org/10.5194/gmd-14-5023-2021.

Waugh, D. W., and D. G. Dritschel, 1999: The dependence of rossby wave breaking on the vertical structure of the polar vortex. *Journal of the atmospheric sciences*, **56 (14)**, 2359–2375, https://doi.org/10.1175/1520-0469(1999)056⟨2359:TDORWB⟩2.0.CO;2.

Whan, K., F. Zwiers, and J. Sillmann, 2016: The influence of atmospheric blocking on extreme winter minimum temperatures in north america. *Journal of Climate*, **29 (12)**, 4361–4381, https://doi.org/10.1175/JCLI-D-15-0493.1.

Williams, K., and Coauthors, 2018: The met office global coupled model 3.0 and 3.1 (gc3. 0 and gc3. 1) configurations. *Journal of Advances in Modeling Earth Systems*, **10 (2)**, 357–380, https://doi.org/10.1002/2017MS001115.

Woollings, T., and Coauthors, 2018: Blocking and its response to climate change. *Current climate change reports*, **4**, 287–300, https://doi.org/10.1007/s40641-018-0108-z.

Yao, Y., D. Luo, A. Dai, and I. Simmonds, 2017: Increased quasi stationarity and persistence of winter ural blocking and eurasian extreme cold events in response to arctic warming. part i: Insights from observational analyses. *Journal of Climate*, **30 (10)**, 3549–3568, https://doi.org/10.1175/JCLI-D-16-0261.1.

1 Appendix A

1.1 TPVTrack Code and Parameters

The default parameters and code for TPVTrack 1.0 can be accessed at `https://github.com/nickszap/tpvTrack`. The parameters updated for the use of this algorithm with ERA5 data are in the my_settings.py script. The updated parameters are as follows:

dFilter = 500.e3

segRestrictPerc = 30.

In the preProcess.py script, 4 lines of code are also added to make the top 4 latitude values equal to fix a problem with the tracker stopping tracks that cross over the pole.

1.2 TempestExtremes

The code and documentation for TempestExtremes tracking algorithm can be accesed at `https://climate.ucdavis.edu/tempestextremes.php`. The commands used to track blocks are as follows:

/tempestextremes/bin/DetectNodes - -in_data (path to blocking index data) - -latname latitude - -lonname longitude - -out control_nodes - -searchbymax (name of blocking index in data) - -minlat 30 - -maxlat 85 - -mergedist 15 - -outputcmd "(name of block index),max,0;(name of DB index),max,0;(name of RI index),max,0"

/tempestextremes/bin/StitchNodes - -in control_nodes - -out control_nodes.csv - -in_fmt "lon,lat,bindex,dbindex,riindex" - -range 18 - -mintime "120h" - -maxgap 2 - -out_file_format "csv"